Quasi-two-dimensional dynamics of plasmas and fluids

Wendell Horton and Akira Hasegawa

Citation: Chaos **4**, 227 (1994); doi: 10.1063/1.166049
View online: http://dx.doi.org/10.1063/1.166049
View Table of Contents: http://scitation.aip.org/content/aip/journal/chaos/4/2?ver=pdfcov
Published by the AIP Publishing

Quasi-two-dimensional dynamics of plasmas and fluids

Wendell Horton
Institute for Fusion Studies and Department of Physics, The University of Texas at Austin, Austin, Texas 78712

Akira Hasegawa
Department of Communication Engineering, Osaka University 2−1 Yamadaoka, Suita 565, Japan

(Received 2 February 1994; accepted for publication 11 April 1994)

In the lowest order of approximation quasi-two-dimensional dynamics of planetary atmospheres and of plasmas in a magnetic field can be described by a common convective vortex equation, the Charney and Hasegawa–Mima (CHM) equation. In contrast to the two-dimensional Navier–Stokes equation, the CHM equation admits "shielded vortex solutions" in a homogeneous limit and linear waves ("Rossby waves" in the planetary atmosphere and "drift waves" in plasmas) in the presence of inhomogeneity. Because of these properties, the nonlinear dynamics described by the CHM equation provide rich solutions which involve turbulent, coherent and wave behaviors. Bringing in nonideal effects such as resistivity makes the plasma equation significantly different from the atmospheric equation with such new effects as instability of the drift wave driven by the resistivity and density gradient. The model equation deviates from the CHM equation and becomes coupled with Maxwell equations. This article reviews the linear and nonlinear dynamics of the quasi-two-dimensional aspect of plasmas and planetary atmosphere starting from the introduction of the ideal model equation (CHM equation) and extending into the most recent progress in plasma turbulence.

TABLE OF CONTENTS

I. INTRODUCTION

Spectral measurements in the tokamak plasma by microwave and laser scattering in the period 1976–1978 revealed for the first time a strong low frequency plasma turbulent characteristic in that the frequency spectral width $\Delta\omega$ of the plasma waves was greater than the mean frequency $\langle\omega\rangle$. The scattering experiments showed that the plasma turbulence spectral width $\Delta\omega$ is comparable or larger than the mean frequency at the spectral peak $\langle\omega\rangle$, i.e., $\Delta\omega > \langle\omega\rangle$ while the level of the plasma turbulence $\sqrt{\langle\delta n^2\rangle}/n_0 \ll 1$ [Mazzucato (1976, 1978), Surko and Slusher (1976, 1978)] remains low. This result initiated the necessity of theoretical interpretation beyond the level of the weak turbulence theory hitherto commonly accepted as a standard approach for plasma turbulence [Sagdeev and Galeev (1968)]. As an attempt to solve this problem Hasegawa and Mima (1977, 1978) came up with a model equation which explains the production of strong turbulence signatures even at the low fluctuation levels $\sqrt{\langle\delta n^2\rangle}/n_0 \cong \nabla \ln n_0(x)/\langle k\rangle \ll 1$, where $n_0(x)$ is the background plasma density and $\langle k\rangle$ is the average wave number. Later it was shown [Hasegawa, Maclennan, and Kodama (1979)] that in the inviscid limit, the Hasegawa–Mima equation has a structure identical to that of the nonlinear Rossby wave derived by Charney (1948) for atmospheric motion of

 1054-1500/94/4(2)/227/25/$6.00

the planetary atmosphere. In the inviscid limit these equations have a feature similar to the two-dimensional Navier–Stokes equation in that they have two conserved quantities, energy and enstrophy, creating the possibility of negative temperature for the modal energy [Onsager (1949)]. In the presence of viscous dissipation this feature induces an inverse cascade of the spectrum [Kraichnan (1967)]. However, the inhomogeneity which brings in the wave character of the CHM dynamics provides an interesting modification to the cascade process [Hasegawa, Maclennan, and Kodama (1979)] because of the interplay with the weak turbulence characteristics such as the conservation of wave quanta.

In addition to the turbulent nature, the inviscid CHM equation admits coherent (vortex) solutions of various types [Larichev and Reznik (1976); Flierl *et al.* (1980); Zabusky and McWilliams (1982)]; which are relatively robust against various perturbations.

Connection of the drift wave instability [Rudakov and Sagdeev (1961)] and the Hasegawa–Mima equation can be made by bringing in nonadiabatic dynamics of electrons either through the Landau damping [Horton (1976, 1986)] or through finite parallel resistivity [Wakatani and Hasegawa (1984)]. The turbulence is then naturally generated without an artificial source, and stationary spectra and self-organization appear [Hasegawa and Wakatani (1983,1987), Horton (1989)].

This review consists of the following sections. Section II gives the derivation of the drift wave equation known as the Hasegawa–Mima equation and the Rossby wave equation known as the Charney equation: we call the common result the CHM equation. Section III describes some general properties of the CHM equation for the inviscid limit such as its statistical property based on spectral as well as its coherent property in the form of certain vortex solutions. Section IV presents the spectral nature of the turbulence in Rossby and drift wave systems. Section V treats the self-organization process of the turbulent structure in real space into vortex structures and discusses the stability of the vortices, the effects of inhomogeneities, and the coupling between the small-scale wave turbulence and the large-scale vortices.

II. DERIVATION OF MODEL EQUATIONS

A. Hasegawa–Mima equation for drift wave

Consider an electrostatic wave at a frequency ω much smaller than the ion cyclotron frequency ω_{ci} in a magnetized (with magnetic field $B_0\hat{\mathbf{z}}$) and inhomogeneous [with density $n_0(x)$] plasma. A linear wave is known to exist in such a plasma if the phase velocity in the direction of the magnetic field, ω/k_z, is between the electron and the ion thermal speed, v_{Te} and v_{Ti}. At long wavelengths the dispersion relation of the wave is given by $\omega=\mathbf{k}\cdot\mathbf{v}_d$, where $\mathbf{v}_d$ is the diamagnetic drift velocity; the wave is called a drift wave [Rudakov and Sagdeev (1961)]. It is sometimes called a universal mode because it is always excited by Čerenkov emission of electrons and is considered to play a crucial role in the magnetic confinement of a plasma. Extensive experimental studies of the turbulent fluctuations associated with various forms of the drift wave instability have been performed in the TEXT tokamak as reviewed by Horton (1990). Other magnetic confinement geometries such as the heliotron/torsatron show similar fluctuations and the associated anomalous transport processes. One of the most important types of drift wave instabilities is driven by the ion temperature gradient [Horton, Choi, and Tang (1981)], and is the plasma physics analogy of the thermal baroclinic instability arising from the preferential solar heating of the low latitude planetary atmosphere that produces the latitudinal temperature gradient [Pedlosky (1987)].

Dropping the ion thermal balance equation eliminates the ion temperature gradient instability which is currently under active investigation with large-scale computer simulation [Horton, Wakatani, and Wootton (1994)].

For the sake of comparison with Rossby wave, it is convenient to assume that the ion temperature is much smaller than the electron temperature $T_i \ll T_e$. For the drift wave description it is convenient to assume that the ion temperature is much smaller than the electron temperature. For the drift wave description, it is convenient to introduce the small expansion parameter ε,

$$\varepsilon=\frac{1}{\omega_{ci}}\frac{\partial}{\partial t}\approx\frac{1}{k_z v_{Te}}\frac{\partial}{\partial t}\approx\rho_s\left|\nabla\left(\ln\frac{n_0}{B_0}\right)\right|\approx\frac{\Omega}{\omega_{ci}}, \tag{2.1}$$

where $\mathbf{\Omega}=\nabla\times\mathbf{v}$ is the vorticity of the ion fluid. The characteristic wave dispersion scale length is

$$\rho_s=\left(\frac{T_e}{m_i}\right)^{1/2}(\omega_{ci})^{-1}=\frac{c(m_i T_e)^{1/2}}{eB}, \tag{2.2}$$

where T_e is the electron temperature, m_i is the ion mass, and $\mathbf{v}$ is the velocity field of ions.

The equations to describe the ion dynamics are the Lorentz equation of motion for the cold ion fluid in an electrostatic field, $\mathbf{E}=-\nabla\phi$

$$\frac{d\mathbf{v}}{dt}=-\frac{e}{m_i}\nabla\phi+\mathbf{v}\times\boldsymbol{\omega}_{ci}, \tag{2.3}$$

and the equation for the number density $n(\mathbf{x}, t)$ conservation of the ions can be written as

$$\nabla\cdot\mathbf{v}=-\frac{d}{dt}\ln n, \tag{2.4}$$

where $\mathbf{v}$ is the ion fluid velocity m_i is the ion mass, e is the electric charge of the ion, ϕ is the electrostatic potential, and $\omega_{ci}(x)\hat{\mathbf{z}}$ is the vector ion cyclotron frequency.

The quasineutrality condition relates the ion density n to the electron density n_e which can be shown to obey the Boltzmann distribution

$$n\simeq n_e=n_0(x)\exp\left(\frac{e\phi}{T_e}\right), \tag{2.5}$$

within the framework of the small parameter, Eq. (2.1). From Eqs. (2.4) and (2.5) we have

$$\nabla\cdot\mathbf{v}=-\frac{d}{dt}\left(\ln n_0+\frac{e\phi}{T_e}\right). \tag{2.6}$$

Since the drift wave is basically a vortex mode, we construct an equation for the vorticity $\Omega(\equiv\nabla\times\mathbf{v})$ by taking the curl of Eq. (2.3). If we note that

$$\frac{d\mathbf{v}}{dt}=\frac{\partial\mathbf{v}}{\partial t}+(\mathbf{v}\cdot\nabla)\mathbf{v}=\frac{\partial\mathbf{v}}{\partial t}+\frac{1}{2}\nabla\mathbf{v}^2-\mathbf{v}\times\Omega$$

and

$$\nabla\times(\mathbf{v}\times\Omega)=-\Omega\nabla\cdot\mathbf{v}+(\Omega\cdot\nabla)\mathbf{v}-(\mathbf{v}\cdot\nabla)\Omega$$
$$=-\Omega\nabla_\perp\cdot\mathbf{v}_\perp-(\mathbf{v}\cdot\nabla)\Omega,$$

we have

$$\frac{d}{dt}(\Omega+\omega_{ci})+(\Omega+\omega_{ci})\nabla_\perp\cdot\mathbf{v}_\perp=0. \tag{2.7}$$

Here the subscript $\perp$ indicates the components perpendicular to the direction of the magnetic field, $\hat{\mathbf{z}}$. Now, we assume a pseudo-three-dimensional situation such that

$$\left|\frac{\partial\mathbf{v}_z}{\partial z}\right|=\varepsilon|\nabla_\perp\cdot\mathbf{v}_\perp|. \tag{2.8}$$

where ε is the small expansion parameter. This assumption is consistent with the condition of the existence of the drift wave. Physically, the assumption means that the ion inertia in the direction of the ambient magnetic field is negligible.

Equation (2.6) is then approximated by

$$\nabla_\perp\cdot\mathbf{v}_\perp=-\frac{d}{dt}\left(\ln n_0+\frac{e\phi}{T_e}\right). \tag{2.9}$$

If we substitute Eq. (2.9) into Eq. (2.7) and use the small parameter expansion of Eq. (2.1), we have

$$\frac{d}{dt}\left[\ln\left(\frac{\omega_{ci}+\Omega}{n_0\exp(e\phi/T_e)}\right)\right]\simeq\frac{d}{dt}\left[\ln\left(\frac{\omega_{ci}}{n_0}\right)+\frac{\Omega}{\omega_{ci}}-\frac{e\phi}{T_e}\right]=0. \tag{2.10}$$

Here if we use the ordering of Eq. (2.1) the vorticity $\boldsymbol{\Omega}\cdot\hat{\mathbf{z}}$ is given by the $\mathbf{E}\times\mathbf{B}$ drift,

$$\boldsymbol{\Omega}=(\nabla\times\mathbf{v}_\perp)\cdot\hat{\mathbf{z}}=\hat{\mathbf{z}}\cdot\nabla\times\left(\frac{\nabla\phi\times\hat{\mathbf{z}}}{B_0}\right)=\frac{1}{B_0}\nabla^2\phi \tag{2.11}$$

and

$$\frac{d}{dt}=\frac{\partial}{\partial t}-\frac{\nabla\phi\times\hat{\mathbf{z}}}{B_0}\cdot\nabla. \tag{2.12}$$

Equations (2.10), (2.11), and (2.12) form a closed set for the electrostatic potential ϕ.

In a low pressure plasma ($\beta=8\pi p/B^2\ll1$), the inhomogeneity in the magnetic field is regarded as small compared with that of the plasma density. If we take ω_{ci} to be approximately constant and use the following normalizations for time, space, and ϕ,

$$\omega_{ci}t\equiv t, \tag{2.13}$$

$$\frac{x,y}{\rho_s}\equiv x,y, \tag{2.14}$$

$$\frac{e\phi}{T_e}\equiv\phi, \tag{2.15}$$

then Eqs. (2.10), (2.11), and (2.12) reduce to

$$\frac{\partial}{\partial t}(\nabla^2\phi-\phi)-[(\nabla\phi\times\hat{\mathbf{z}})\cdot\nabla]\left[\nabla^2\phi-\ln\left(\frac{n_0}{\omega_{ci}}\right)\right]=0, \tag{2.16}$$

which is the equation derived by Hasegawa and Mima [Hasegawa and Mima (1978)]. Here, we suppressed the subscript $\perp$ in the gradient operator ∇; that is ∇ means

$$\nabla=\hat{\mathbf{x}}\frac{\partial}{\partial x}+\hat{\mathbf{y}}\frac{\partial}{\partial y}.$$

We note here that in a homogeneous case this expression, Eq. (2.16), closely resembles that for the streamfunction ψ of the two-dimensional Euler equation for an incompressible fluid, which, in a homogeneous fluid, can be written

$$\frac{\partial}{\partial t}(\nabla^2\psi)-[(\nabla\psi\times\hat{\mathbf{z}})\cdot\nabla]\nabla^2\psi=0. \tag{2.17}$$

That is, Eq. (2.17) is the rotational part of the Euler equation $\rho d\mathbf{v}/dt=-\nabla p$ for constant mass density ρ and $\mathbf{v}=\hat{\mathbf{z}}\times\nabla\psi$. Equation (2.16) reduces to Eq. (2.17) when $\nabla^2\phi/\phi\to\infty$ and $n_0/\omega_{ci}=$constant.

There exist two fundamental differences between these two equations (2.16) and (2.17). First, the 2-D incompressible Euler's equation (2.17) does not have a characteristic spatial scale, while the spatial scale of the Hasegawa–Mima equation is given by ρ_s in Eq. (2.2) [which is the unit length in Eq. (2.16)]. The absence of a scale length in the Euler equation yields scale invariant turbulent spectra whereas the CHM equation has a break in the wave-number spectrum as shown in Sec. IV C. Second, the fluid motion of the Hasegawa–Mima equation is not divergence-free. There exists a sink or a source in the x-y plane which is due to the implicit connection of the fluid in the z direction. The connection with the z flow in the direction parallel to the magnetic field is taken into account by Eq. (2.5) which requires $k_z v_e\gg\omega$ as expressed in Eq. (2.1).

In the presence of an inhomogeneity, the Hasegawa–Mima equation admits a linear wave whose dispersion relation is given by

$$\omega=\omega_{\mathbf{k}}=-[(\mathbf{k}\times\hat{\mathbf{z}})\cdot\nabla\ln n_0]/(1+k^2)=\frac{\omega_*}{(1+k^2)}, \tag{2.18}$$

where $\mathbf{k}$ is the wave vector in the direction perpendicular to $\hat{\mathbf{z}}$. This frequency $\omega_{\mathbf{k}}$ is the well-known drift wave frequency and follows for solutions $\phi_{\mathbf{k}}e^{i\mathbf{k}\cdot\mathbf{x}-i\omega t}+$c.c. of Eq. (2.16) when $\nabla\phi\times\hat{\mathbf{z}}\cdot\nabla\nabla^2\phi=\hat{\mathbf{z}}\cdot\nabla\tilde{\phi}\times\nabla\nabla^2\phi_k\sim k^4\phi_k^2$ terms is negligible compared with $\omega_*\phi_{\mathbf{k}}$. At long wavelengths $k^2\ll1$, the wave packet propagates with weak dispersion at the speed $\mathbf{v}_d$ and the frequency $\omega_{\mathbf{k}}=\mathbf{k}\cdot\mathbf{v}_d\equiv\omega_*$ where $\mathbf{v}_d=\hat{\mathbf{z}}\times\nabla\ln n_0(cT_e/eB)$. The typical size of the time and space parameters in a tokamak plasma are

$$\omega_{ci}\approx10^8\sim10^9\ \mathrm{s}^{-1},$$

$$\omega^*\approx10^5\sim10^7\ \mathrm{s}^{-1},$$

$$\rho_s\approx10^{-3}\ \mathrm{m}.$$

TABLE I. Plasma drift wave parameters.

	PLT [Brower *et al.* (1985)]	TEXT [Mazzucato (1982)]
Magnetic field	3 T	2 T
Electron temperature	1 keV	500 eV
Density n_e and	2×10^{13} cm^{-3}	3×10^{13} cm^{-3}
gradient length L_n	20 cm	10 cm
Drift velocity v_d	2×10^5 cm/s	1×10^5 cm/s
k scattering experiment	5–20 cm^{-1}	1.5–15 cm^{-1}
ω scattering experiment	50–500 kHz	100–1000 kHz
$\tilde{n}_e/n_e$	5×10^{-3} to 0.02	0.01 to 0.1

The size of the nonlinearities $e\phi/T_e$ and Ω/ω_{ci} as measured by laser scattering [Surko and Slusher (1976), and Slusher and Surko (1978)] and microwave scattering [Mazzucato (1976)] from a tokamak plasma are

$$\frac{e\phi}{T_e}\approx10^{-2}\sim10^{-1},$$

$$\frac{\Omega}{\omega_{ci}}=k^2\rho_s^2\left(\frac{e\phi}{T_e}\right)\approx10^{-3}\sim10^{-2}.$$

More recent measurements on larger tokamaks confirm these values showing that the small levels of $e\phi/T_e$ occur in the interior and the large values in the edge of the confined plasma. The system parameters and the drift wave fluctuation properties determined from the electromagnetic scattering experiment by Mazzucato (1982) in the Princeton Large Torus (PLT) and by Brower *et al.* (1985) in the Texas Experimental (TEXT) are given in Table I.

B. Charney equation for the Rossby wave

There exists a wave in the atmospheric pressure system which is almost identical in its properties to the drift wave. The wave is called a "Rossby wave," and it propagates longitudinally with a speed proportional to the gradient of the Coriolis force.

Let us consider the atmospheric motion on the surface of a rotating planet. The two-dimensional velocity $\mathbf{v}$ of the atmospheric flow in the horizontal plane obeys the equation of motion [Morikawa (1960)],

$$\frac{d\mathbf{v}}{dt}=-g\nabla H+f\mathbf{v}\times\hat{\mathbf{z}}, \tag{2.19}$$

where ∇ is the gradient in the horizontal plane, f is the Coriolis parameter, x represents the north–south direction, H is the surface displacement of the atmosphere in the vertical ($\hat{\mathbf{z}}$) direction, and g is the constant of gravity. Equation (2.19) describes the horizontal acceleration of the constant mass density fluid by the gradient of the hydrostatic pressure $p=\rho gH$ and the Coriolis force $2\boldsymbol{\Omega}\times\mathbf{v}$ from being in a rotating frame of reference with angular velocity $\boldsymbol{\Omega}$. The quantity H also represents the surface density of the atmosphere; hence, it obeys the continuity equation,

$$\nabla\cdot\mathbf{v}=-\frac{d}{dt}\ln H \tag{2.20}$$

where ∇ is again the two-dimensional operator in the x-y plane and H is the total depth of the atmosphere

$$H=H_0+h, \tag{2.21}$$

and H_0 is the average depth. We see immediately the close resemblance of Eqs. (2.19) and (2.20) to Eqs. (2.3) and (2.4). In fact, they are identical if $h\ll H_0$, and when f is replaced by ω_{ci}, and h by ϕ. The only difference is that the spatial variation of f is generally larger than that of H_0.

If we introduce a small parameter called the Rossby number,

$$\varepsilon=\frac{1}{\langle f\rangle}\frac{\partial}{\partial t}\approx\frac{\Omega}{\langle f\rangle}\approx\left|\rho_g\nabla\ln\frac{H_0}{f}\right|, \tag{2.22}$$

and introduce the following scaling:

$$\langle f\rangle t\equiv t, \tag{2.23}$$

$$\frac{(x,y)}{\rho_g}\equiv x,y, \tag{2.24}$$

$$\frac{h}{H_0}\equiv h, \tag{2.25}$$

where the spatial scale ρ_g (Rossby radius) is given by

$$\rho_g=\frac{(gH_0)^{1/2}}{\langle f\rangle}, \tag{2.26}$$

and $\langle f\rangle$ is the average of f, Eqs. (2.19) and (2.21) can be reduced to the form of Eq. (2.16) [Charney (1948)]

$$\frac{\partial}{\partial t}(\nabla^2h-h)-[(\nabla h\times\hat{\mathbf{z}})\cdot\nabla]\left(\nabla^2h-\ln\frac{H_0}{f}\right)=0. \tag{2.27}$$

The linearized solution gives the dispersion relation for

$$\omega_{\mathbf{k}}=\frac{[(\mathbf{k}\times\hat{\mathbf{z}})\cdot\nabla\ln f]}{(1+k^2)}$$

$$=\frac{\mathbf{k}\cdot\mathbf{v}_R}{1+k^2}. \tag{2.28}$$

Equation (2.28) defines the Rossby velocity $\mathbf{v}_R=\hat{\mathbf{z}}\times\nabla\ln f$ in units of $c_g=\rho_g\langle f\rangle=(gH_0)^{1/2}$ which is the isothermal sound speed c_s in the atmosphere. Stewart (1943) and Morikawa (1960) have studied the nonlinear dynamics of Rossby waves in terms on interacting vortices (geostrophic vortices) using Eqs. (2.16) and (2.17) in a uniform fluid. Typical parameters in the Earth's atmospheric system in the mid-latitude are

$$H_0\approx8\times10^3\ \text{m},\quad \rho_g\approx2\times10^6\ \text{m},$$

$$\langle f\rangle\approx1.6\times10^{-4}\ \text{s}^{-1},\quad \frac{\omega_R}{f}\approx10^{-1}.$$

Unlike the case of a magnetized plasma, where the finite ion gyroradius ρ_i effects at scales $k^{-1}\approx\rho_i=(T_i/T_e)^{1/2}\rho_s$ disallow the use of a simplified fluid expression for $k\rho_s\gg1$ (if $T_i\approx T_e$) in the case of geostrophic turbulence $k\rho_s$ can become very large. At sufficiently large $k\rho_s$ the dynamics of Eq. (2.27) reduces to that of the Euler equation given in Eq. (2.17).

TABLE II. Analogy between drift wave and Rossby wave.

Drift wave	Rossby Wave
HM equation	Charney equation
$(1-\nabla^2)\frac{\partial\phi}{\partial t}+v_d\frac{\partial\phi}{\partial y}-[\phi,\nabla^2\phi]=0$	$(1-\nabla^2)\frac{\partial g}{\partial t}+v_R\frac{\partial h}{\partial y}-[h,\nabla^2 h]=0$
Electrostatic potential $\phi(x,y,t)$	Variable part of fluid depth: $h(x,y,t)$
$\phi(x,y,t)=\left(\frac{L_n}{\rho_s}\right)e\Phi\left(\frac{x}{\rho_s},\frac{y}{\rho_s},\frac{c_s}{r_n}t\right)\Big/T_e$	$h(x,y,t)=\left(\frac{L_R}{\rho_g}\right)\delta H\left(\frac{x}{\rho_g},\frac{y}{\rho_g},\frac{c_g}{L_R}t\right)\Big/H$
Lorentz force: $m\omega_{ci}\mathbf{v}_\perp\times\hat{\mathbf{z}}$	Coriolis force: $\rho f\,\mathbf{v}_\perp\times\hat{\mathbf{z}}$
$\mathbf{E}\times\mathbf{B}$ drift flow: $\mathbf{v}_\perp=(c/B)\,\hat{\mathbf{z}}\times\nabla\Phi$	Geostrophic flow: $\mathbf{v}_\perp=\left(\frac{g}{f}\right)\hat{z}\times\nabla\partial h$
Cyclotron frequency: $\omega_{ci}=\frac{eB}{cm_i}$	Coriolis parameter: f
Drift coefficient: $L_n^{-1}=-\frac{\partial}{\partial x}\ln n_0$	Rossby coefficient: $L_R^{-1}=\frac{\partial}{\partial x}\ln\left(\frac{f}{H}\right)$
Larmor radius: $\rho_s=\frac{c_s}{\omega_{ci}}$	Rossby radius: $\rho_g=\frac{c_g}{f}$
Ion-acoustic speed: $c_s=\left(\frac{T_e}{m_i}\right)^{1/2}$	Gravity wave speed: $c_g=(gH)^{1/2}$
where T_e is electron temperature	where H is depth of fluid layer
Drift velocity: $v_d=c_s\rho_s\frac{\partial}{\partial x}\ln n_0$	Rossby velocity: $v_R=c_g g\frac{\partial}{\partial x}\ln\left(\frac{f}{H}\right)$
Dispersion relation: $\omega=\frac{k_y v_d}{1+k^2\rho_s^2}$	Dispersion relation: $\omega=\frac{k_y v_R}{1+k^2\rho_g^2}$

Other than this point, we can see the close similarity between the drift wave and the Rossby wave. The comparisons between the plasma wave and the geophysical wave are summarized in Table II.

III. INVISCID PROPERTIES OF CHARNEY AND HASEGAWA–MIMA EQUATIONS

A. Conservation laws and spectral distribution

To consider the turbulence which can be described by the Charney and Hasegawa–Mima equation (CHM) it is convenient to review some of the properties of this equation. First, it can easily be shown [Hasegawa and Mima (1978)] that these equations contain two fundamental conserved quantities; the total energy W,

$$\frac{\partial W}{\partial t}\equiv\frac{\partial}{\partial t}\frac{1}{2}\int[(\nabla\phi)^2+\phi^2]\,dV=0, \tag{3.1}$$

and the (potential) enstrophy U,

$$\frac{\partial U}{\partial t}=\frac{\partial}{\partial t}\frac{1}{2}\int[(\nabla\phi)^2+(\nabla^2\phi)^2]dV=0, \tag{3.2}$$

where $\int dV$ is the volume integral. Using these conserved quantities, a stationary spectrum $\langle|\phi_k|^2\rangle$ for the conservative (dissipationless) system has been obtained [Hasegawa *et al.* (1978)]

$$\langle|\phi_k|^2\rangle=(1+k^2)^{-1}(\alpha+\beta k^2)^{-1}. \tag{3.3}$$

Hence, the energy spectrum becomes

$$W_k=(1+k^2)\langle|\phi_k^2|\rangle=\frac{1}{\alpha+\beta k^2} \tag{3.4}$$

and is the same as for the case of the two-dimensional Euler equation [Onsager (1949)]. If $\alpha\beta<0$, the spectrum indicates a negative temperature state and condensation at small k values.

B. Single vortex solutions

Assuming a certain rigidity of the vortices, Steward (1943) and Morikawa (1960) study interactions among vortex solutions of Eq. (2.16) without the inhomogeneous term. The formulation is similar to the two-dimensional vortex solutions. The solution can be written

$$\phi=\sum_j\omega_j K_0[|\mathbf{r}-\mathbf{r}_j(t)|] \tag{3.5}$$

and

$$\frac{d\mathbf{r}_j}{dt}=-\nabla\phi\times\hat{\mathbf{z}}, \tag{3.6}$$

where K_0 is the modified Bessel function of the second kind, and ω_j is the circulation.

In contrast, the two-dimensional Euler's vortex solution is $\phi=\Sigma_j\omega_j\ln|\mathbf{r}-\mathbf{r}_j|$. If $|\mathbf{r}-\mathbf{r}_i|\ll 1$, these two solutions are the same, but Stewart's vortex dies off exponentially at $|\mathbf{r}-\mathbf{r}_i|\gg 1$, hence, it can be considered as a shielded vortex. This means that the vortex of Eq. (2.16) has a finite size given by ρ_s for ρ_g. This exponential shielding has a significant effect on the convection.

The interacting N vortices of the homogeneous Hasegawa–Mima equation can be described by the Hamiltonian,

$$H=\sum_{i>j}^{N}\sum^{N}\ \omega_i\omega_j K_0(|\mathbf{r}_i-\mathbf{r}_j|); \tag{3.7}$$

here, the canonical variables are the x and y coordinates of the centers of the vortices, x_i, y_i. The Hamiltonian equations of motion for these centers $\mathbf{r}_i(t)=(x_i, y_i)$ are

$$\frac{\partial H}{\partial x_i}=\omega_i\frac{dy_i}{dt}\,,\quad \frac{\partial H}{\partial y_i}=-\omega_i\frac{dx_i}{dt}\,. \tag{3.8}$$

If can easily be verified that the following conservation relations exist:

(i) invariance of H:

$$\frac{dH}{dt}=0, \tag{3.9}$$

(ii) stationary mass center:

$$\frac{d}{dt}\sum_i\ \omega_i\mathbf{r}_i=0, \tag{3.10}$$

(iii) conservation of the moment of inertia:

$$\frac{d}{dt}\sum_i\ \omega_i\mathbf{r}_i^2\times\mathbf{v}_i=0, \tag{3.11}$$

We note here that these solutions of interacting vortices break down when the vortex density is increased and the inelastic collision starts to dominate. As the density is further increased, the field becomes turbulent. The chaotic flow fields and the associated transport are investigated by Kono and Horton (1991).

Even in the presence of the inhomogeneity term in Eq. (2.16) vortex solutions can be found by means of the Galilean transformation,

$$y=\eta+\kappa t,\quad \phi=\psi+\kappa x, \tag{3.12}$$

where

$$\boldsymbol{\kappa}=\hat{\mathbf{z}}\times\boldsymbol{\nabla}\ln\left(\frac{\omega_{ci}}{n_0}\right). \tag{3.13}$$

The transformation (3.12) gives

$$\frac{\partial}{\partial t}=\frac{\partial}{\partial t}-\kappa\frac{\partial}{\partial\eta}\,. \tag{3.14}$$

Thus Eq. (2.16) is reduced to a symmetric structure:

$$\frac{\partial}{\partial t}(\nabla^2\psi-\psi)-(\boldsymbol{\nabla}\psi\times\mathbf{z})\cdot\boldsymbol{\nabla}(\nabla^2\psi)=0, \tag{3.15}$$

where $\boldsymbol{\nabla}$ is in the x-η plane. This equation also conserves energy ($\frac{1}{2}\int[(\nabla^2\psi)^2+(\boldsymbol{\nabla}\psi)^2]dV$).

Equation (3.15) admits the single vortex solution of the type (3.5). Now we review the dipolar vortex pair solutions of Eqs. (2.16) and (2.27).

C. Vortex pair solution

In addition to the point vortex solution, the Hasegawa–Mima equation admits a stationary vortex pair solution in a moving coordinate $\eta=y-ut$. The dipolar vortex solution of Eq. (2.16), called modon [Larichev and Reznik (1976)], is given by

$$\phi(r,\theta)=\begin{cases}\dfrac{u+\kappa}{\lambda^2}\left[a\dfrac{J_1(\lambda r)}{J_1(\lambda a)}-r\left(\dfrac{\lambda^2}{\rho^2}+1\right)\right]\sin\theta, & r<a,\\[2ex] \dfrac{u+\kappa}{\rho^2}\,a\,\dfrac{K_1(\rho r)}{K_1(\rho a)}\sin\theta, & r>a,\end{cases} \tag{3.16}$$

where $\phi(x,y,t)=\phi(r\sin\theta, ut+r\cos\theta)$. Here J_1 is the first-order Bessel function of the first kind, K_1 is a first-order modified Bessel function of the second kind, u is the translation speed in the y direction,

$$r=[x^2+(y-ut)^2]^{1/2},$$

ρ is the parameter related to u and κ through

$$u=\frac{\kappa}{\rho^2-1}, \tag{3.17}$$

and a is the radius of a vortex pair within which there exists a constant vorticity. The continuity of $\partial\phi/\partial r$ at $r=a$ gives the eigenvalue for λ,

$$\sum_{n=1}^{\infty}\frac{1}{(\lambda a)^2-\gamma_n^2}=\frac{1}{2\rho a}\left(\frac{1}{\rho a}-\frac{K_1'(\rho a)}{K_1(\rho a)}\right),$$

where γ_n is the monotonically increasing sequence of zeros of $J_1(r)$,

$$J_1(\gamma_n)=0.$$

The streamfunction ϕ for a modon is shown in Fig. 1. The dipole vortex is called the "modon" from the original oceanographic studies. A modon is somewhat similar to the soliton of the Korteweg–de Vries (KdV) equation in that a modon with a larger radius propagates faster and has a large potential difference. Furthermore, stability of modons against some types of collisions has been demonstrated. However, modons, as well as single vortex solutions, are not eigenstates of the vortex equations, that is, they are not integrable. These issues are discussed in Sec. V.

The dipole vortices or modons propagate in regions complementary to those of the waves. This complementarity is shown in terms of the speed u from Eq. (3.17) compared with the wave phase velocities as shown in Fig. 2 from Meiss and Horton (1983) for the case of finite $k_\parallel c_s$ from the ion-acoustic waves. The values of the energy W and enstrophy U integrals are given in Meiss–Horton (1983) as a function of u/v_d and a/ρ_s.

The properties of the dipole vortices have been studied in rotating water tanks by Antipov *et al.* (1982), and Antonova *et al.* (1983) as reviewed by Nezlin (1986). Further studies of the elastic dipole collisions and the existence of tripolar vortices were carried out by Van Heijst (1989) and his collaborators.

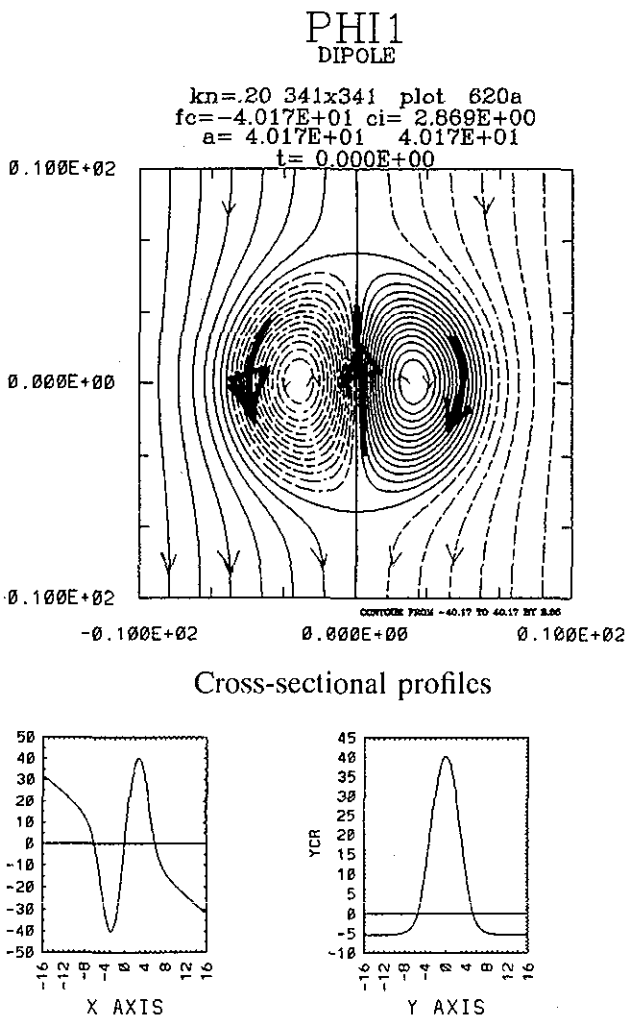

FIG. 1. Isolines of the streamfunction for the Rossby wave or equipotential lines for the drift wave dipole vortex in the frame moving with the vortex. Solid contours are positive potentials and dashed are negative. The vortex parameters are $r_0=a=6\rho_s$ and $u=2v_d$.

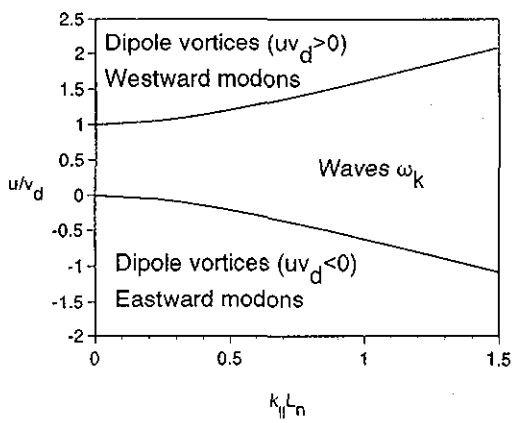

FIG. 2. The complementary propagation regions of the waves and dipole vortices are shown for an example in Meiss–Horton (1983) where there is coupling to the ion-acoustic waves.

D. Mode coupling properties

Here, we consider the turbulence property of the Charney and Hasegawa–Mima equation. It is convenient to consider the dynamic change of the spatial Fourier spectrum. If we write

$$\phi(x,t)=\frac{1}{2}\sum_{\mathbf{k}}\ [\phi_{\mathbf{k}}(t)\ \exp\ (i\mathbf{k}\cdot\mathbf{x})+\text{c.c.}], \tag{3.18}$$

Eq. (2.16) becomes

$$\frac{d\phi_{\mathbf{k}}}{dt}+i\omega_{\mathbf{k}}\phi_{\mathbf{k}}=\sum_{\mathbf{k}+\mathbf{k}'+\mathbf{k}''=0}\Lambda^{\mathbf{k}}_{\mathbf{k}',\mathbf{k}''}\phi^*_{\mathbf{k}'}\phi^*_{\mathbf{k}''}, \tag{3.19}$$

where the asterisk indicates the complex conjugate,

$$\omega_{\mathbf{k}}=\frac{\mathbf{k}\times\hat{\mathbf{z}}\cdot\nabla\ \ln\ (n_0/\omega_{ci})}{1+k^2} \tag{3.20}$$

is the drift or Rossby wave frequency, and the matrix element $\Lambda^{\mathbf{k}}_{\mathbf{k}',\mathbf{k}''}$ is given by

$$\Lambda^{\mathbf{k}}_{\mathbf{k}',\mathbf{k}''}=\frac{1}{2}\frac{1}{1+k^2}\ (\mathbf{k}'\times\mathbf{k}'')\cdot\hat{\mathbf{z}}(k''^2-k'^2). \tag{3.21}$$

Let us consider three plane waves with wave numbers $\mathbf{k}_1$, $\mathbf{k}_2$, and $\mathbf{k}_3$ such that $\mathbf{k}_1+\mathbf{k}_2+\mathbf{k}_3=0$. Let us suppose that those waves have amplitudes larger than other waves in the summation of Eq. (3.19) and study the energy flow among these three waves. Equation (3.19) for the three interacting waves may be written

$$\frac{d\phi_1}{dt}+i\omega_1\phi_1=\Lambda^1_{2,3}\phi^*_2\phi^*_3, \tag{3.22}$$

$$\frac{d\phi_2}{dt}+i\omega_2\phi_2=\Lambda^2_{3,1}\phi^*_3\phi^*_1, \tag{3.23}$$

$$\frac{d\phi_3}{dt}+i\omega_3\phi_3=\Lambda^3_{1,2}\phi^*_1\phi^*_2, \tag{3.24}$$

where

$$\phi_j(t)=\phi_{\mathbf{k}_j}(t), \tag{3.25}$$

and

$$\omega_j=\omega_{\mathbf{k}_j},\ \ j=1,2,3. \tag{3.26}$$

The direction of energy flow or decay may be found by studying the stability of a situation in which one of the modes 1, 2, 3 is more highly populated than others. For this purpose we first assume, without loss of generality, that $k_j\equiv|\mathbf{k}_j|$ such that

$$k_1\leqslant k_2\leqslant k_3. \tag{3.27}$$

We first consider a case in which the k_2 mode is highly populated so that $|\phi_2|\gg|\phi_1|,\ |\phi_3|$. We can then linearize Eqs. (3.22)–(3.24) to give

$$\phi_2=A_2\ \exp\ (-i\omega_2 t),\ \ A_2=\text{const}, \tag{3.28}$$

and

$$\frac{dA_1}{dt}=\Lambda^1_{2,3}A^*_2A^*_3\ \exp\ (i\Delta\omega t), \tag{3.29}$$

$$\frac{dA_3}{dt} = \Lambda^3_{1,2} A^*_2 A^*_1 \exp(i\Delta\omega t), \tag{3.30}$$

with

$$\phi_j \equiv A_j(t) \exp(-i\omega_j t), \quad j = 1,3$$

and

$$\Delta\omega = \omega_1 + \omega_2 + \omega_3, \tag{3.31}$$

is the frequency mismatch.

From Eqs. (3.29) and (3.30), we have

$$\frac{d^2A_1}{dt^2} - i\Delta\omega \frac{dA_1}{dt} - \Lambda^1_{2,3}\Lambda^3_{1,2}|A_2|^2 A_1 = 0. \tag{3.32}$$

Hence, the instability (exponential growth of A_1 and A_3) occurs when

$$\Delta\omega^2 - 4\Lambda^1_{2,3}\Lambda^3_{1,2}|A_2|^2 < 0; \tag{3.33}$$

and the growth rate γ of the daughter waves is given by

$$\gamma = (\Lambda^1_{2,3}\Lambda^3_{1,2}|A_2|^2 - \tfrac{1}{4}\Delta\omega^2)^{1/2}. \tag{3.34}$$

Inequality (3.33) shows that the stability is decided by the sign of the product $\Lambda^1_{2,3}\Lambda^3_{1,2}$.

Now, in view of the assumed relation (3.27), both of the quantities $k_2^2 - k_3^2$ and $k_1^2 - k_2^2$ are negative (or zero) in Eq. (3.21), and $(\mathbf{k}_2 \times \mathbf{k}_3)\cdot\hat{\mathbf{z}}$ and $(\mathbf{k}_1 \times \mathbf{k}_2)\cdot\hat{\mathbf{z}}$ have the same sign (if not zero). Hence $\Lambda^1_{2,3}\Lambda^3_{1,2} > 0$, and this situation can be unstable.

On the other hand, since $\Lambda^2_{3,1}\Lambda^3_{1,2}$ and $\Lambda^2_{2,3}\Lambda^3_{2,1}$ are always negative (or zero), if modes 1 or 3 are highly populated, the system is stable. Hence we conclude that the necessary condition for a spectrum cascade is to excite a shorter and a longer wavelength mode simultaneously. We note here that since this is not a resonant decay, by the time the decay process is completed, many other modes have also been excited.

Let us discuss the conservation of quanta in the decay process. If we introduce a number of quanta of the three waves, defined by

$$N_p = (1 + k_p^2)|\phi_p|^2 / |k_q^2 - k_r^2|, \qquad k_q^2 \neq k_r^2, \tag{3.35}$$

from Eqs. (3.22) to (3.24) we find

$$N_3 - N_1 = \text{const}$$

and

$$N_2 + N_1 = \text{const}, \quad N_2 + N_3 = \text{const}. \tag{3.36}$$

These relations show that a loss of one quantum in N_2 appears as a gain of one quantum in N_1 and N_3, respectively. The quantity N defined in Eq. (3.35) thus serves the role as the number of quanta in the decay process. Since the characteristic frequency of a vortex is zero, the standard definition of a number of quanta, $n_{\mathbf{k}} = W_{\mathbf{k}}/\hbar\omega_{\mathbf{k}}$, only applies in the three-wave resonance limit given in Sec. IV B. The number of quanta N_p defined here has the strange property that it depends on the wave numbers of the other interacting waves.

In a region of small wave numbers ($k^2 \ll 1$), the first term in the growth rate expression, Eq. (3.34), becomes small, and the decay process occurs only when $\Delta\omega \approx 0$, i.e., when the frequency mismatch is small. In this case the resonant three-wave interaction dominates the decay process. The number of quanta defined in Eq. (3.35) reduces to the conventional form because

$$k_q^2 - k_r^2 = k_{qy}/\omega_q - k_{ry}/\omega_r = \omega_p M, \tag{3.37}$$

where

$$M = (3\omega_p\omega_q\omega_r)^{-1}[\omega_p(k_{ry} - k_{qy}) + \omega_q(k_{py} - k_{ry}) + \omega_r(k_{qy} - k_{py})] \tag{3.38}$$

and k_y is the component of the $\mathbf{k}$ vector in the direction of $\hat{\mathbf{z}} \times \nabla \ln n_0$. Equation (3.37) with Eq. (3.35) gives $N_p \propto n_p = W_p/\hbar\omega_p$. Hence, in the long wavelength region, decay occurs from the highest frequency mode to two lower frequency modes.

Now, the energy W_k of the $\mathbf{k}$ mode is given by $W_k = |\phi_k|^2(1 + k^2)$. Hence, from Eqs. (3.35) and (3.36), we see that the partition of energy to modes 1 and 3, from the loss of a unit of energy $\Delta W_2 = -1$ from mode 2 is given by

$$\Delta W_1 = \frac{k_3^2 - k_2^2}{k_3^2 - k_1^2}, \quad \Delta W_3 = \frac{k_2^2 - k_1^2}{k_3^2 - k_1^2}. \tag{3.39}$$

In summary, the cascade occurs from the wave with wave number k_2 such that $k_1 < k_2 < k_3$ to waves with wave number k_1 and k_3. If the frequency mismatch, $\Delta\omega = \omega_1 + \omega_2 + \omega_3$, is zero, the cascade occurs from the wave with the highest frequency $\omega_2 (= -\omega_1 - \omega_3)$ to waves with lower frequencies ω_1 and ω_3.

E. The inverse cascade

The mathematical description of a fully developed turbulent state is difficult, if not impossible. However, the turbulent spectrum in the inertial range may be obtained by using an argument based on the Kolmogorov law. [Recall that the inertial range is a range in wave-number space where there is neither a source nor a sink (dissipation) and where the wave-number spectrum is assumed to cascade smoothly in a statistically stationary state.]

The Kolmogorov hypothesis is based on an isotropic, homogeneous turbulence in which there is a local transfer of turbulent energy between neighboring k scales.

If we write the Fourier amplitude of the velocity field as $v_{\mathbf{k}}$, the rate at which the spectrum cascades is given by $kv_{\mathbf{k}}$ [the second term in Eq. (2.17)]. The omnidirectional energy spectrum $W(k)$ is defined such that $\int_0^\infty W(k)dk$ gives the total energy, where $k = (\mathbf{k}\cdot\mathbf{k})^{1/2}$. Hence $W(k)k$ has the dimension of $v_{\mathbf{k}}^2$. Kolmogorov (1941) argues that, in a quasi-steady state, there should be a stationary flow of energy in $\mathbf{k}$ space from the source to the sink. This means that the energy density flow $\rho k v_k \, v_k^2$ should be constant and given by the dissipation rate of the energy density at the sink:

$$\rho k v_k^3 = \varepsilon. \tag{3.40}$$

Writing $v_k = [kW(k)]^{1/2}$, $W(k)$ is given by

$$W(k) = C\left(\frac{\varepsilon}{\rho}\right)^{2/3} k^{-5/3}, \tag{3.41}$$

where C is a universal dimensionless constant. In three- (or one-) dimensional turbulence, only the energy is conserved in the inertial range, and the energy spectrum cascades toward large wave numbers where it is dissipated because of the viscosity. Equation (3.41) is the famous Kolmogorov spectrum [Kolmogorov (1941)].

Now, in two-dimensional turbulence there is an additional conserved quantity, the enstrophy. Hence two types of inertial ranges are expected, one for energy and the other for enstrophy. Since the enstrophy density is given by $\rho k^2 v_k^2$, the inertial range of enstrophy requires that

$$\rho k v_k k^2 v_k^2 = \varepsilon' = \text{const.} \tag{3.42}$$

Thus, writing $v_k = [kW(k)]^{1/2}$, the energy spectrum in this range is given by

$$W(k) = C' \left(\frac{\varepsilon'}{\rho} \right)^{2/3} k^{-3}. \tag{3.43}$$

Equation (3.43) shows an energy spectrum of k^{-3}, in contrast to the Kolmogorov spectrum of $k^{-5/3}$, which is obtained from the inertial range of energy. Kraichnan (1967) showed that if $W(k) \sim k^{-3}$ [more precisely, $W(k) \sim k^{-3} (\ln k)^{-1/3}$] there is no energy cascade, while if $W(k) \sim k^{-5/3}$, there is no enstrophy cascade. Hence a source at $k = k_s$ will set up two inertial ranges, $k > k_s$ and $k < k_s$. Since the enstrophy, because of its larger k dependence, is dissipated at large wave numbers at a rate faster than the energy, the $k > k_s$ region is expected to be the inertial range for enstrophy, which implies that the $k < k_s$ region would be inertial range for energy. Thus the energy spectrum has two parts:

$$W(k) \sim k^{-3}, \qquad k > k_s, \tag{3.44}$$

$$W(k) \sim k^{-5/3}, \qquad k < k_s. \tag{3.45}$$

Kraichnan argues that since there is no energy cascade for $k > k_s$, the energy should cascade toward the smaller wave numbers for $k < k_s$. In other words an inverse cascade is expected. On the other hand, the enstrophy cascades toward the large-wave-number regime at $k > k_s$. However, in the absence of energy dissipation in the small wave number regime, it is difficult to see how an inertial range for energy could be established if $k < k_s$. Hence let us investigate the question of the inverse cascade without making any assumption about the inertial range spectrum. First, we consider the following thought experiment. Imagine a source at say, $k = k_s$, with energy W_s. Through mode–mode coupling this would decay to two modes with wave numbers $\mathbf{k}_1$ and $\mathbf{k}_2$.

Let us suppose, for simplicity, that the cascade to two wave numbers occurs at each step such that the decay rate is maximized. This condition can be found by maximizing the product $\Lambda^{\mathbf{k}_1}_{\mathbf{k}_2\mathbf{k}_s} \Lambda^{\mathbf{k}_2}_{\mathbf{k}_s\mathbf{k}_1}$, and is given by $k_2^2 = k_s^2 + k_1^2$, $k_1^2 = (\sqrt{2}-1) k_s^2$ (so $k_2^2 = \sqrt{2} k_s^2$). We denote this ratio of wave numbers squared by $p (= k_1^2/k_s^2 = \sqrt{2}-1)$, and see how the cascade proceeds to form the energy spectrum.

We have seen that the k_s^2 first decays to wave numbers at $k_1^2 = p k_s^2$ and $k_2^2 = (1+p) k_s^2$, with a corresponding energy partition, given by Eqs. (3.39), into $W_1 = p W_s$ and $(1-p) W_s$. In the next step of the cascade, the mode at k_1 decays to a mode at $p k_1^2 = p^2 k_s^2$ and $(1+p)\, k_1^2 = p(1+p)\, k_s^2$, while the mode at k_2^2 decays to $p k_2^2 = p(1+p) k_s^2$ and $(1+p) k_2^2 = (1+p)^2 k_s^2$. The corresponding energy partitions are $p^2 W_s$, $2p(1-p) W_s$ and $(1-p)^2 W_s$ for squared wave numbers at $p^2 k_s^2$, $p(1+p) k_s^2$ and $(1+p) k_s^2$, respectively. Continuing to the nth step, we see that the energy distribution is given by a binomial distribution for a parameter r/n which is related to the value of k^2 in the following manner:

$$W[k^2 = p^{n-r} (1+p)^r k_s^2] = \binom{n}{r} p^{n-r} (1-p)^r W_s. \tag{3.46}$$

Equation (3.46) gives the energy spectrum which results from a series of cascades at a fixed ratio of k_1^2/k_p^2 at each step, where $k_1^2 + k_s^2 = k_2^2$. Energy conservation is given by

$$\sum_{r=0}^{n} \binom{n}{r} p^{n-r} (1-p)^r = 1.$$

We now show that the energy spectrum condenses at $k \to 0$ as $n \to \infty$. First we note that the peak of a binomial distribution occurs at $r/n \to 1-p$ as $n \to \infty$. Hence let us evaluate the wave number $k^2 = k_p^2$ which corresponds to the peak of the distribution as $n \to \infty$. From Eq. (3.46)

$$k_p^2 = \lim_{n\to\infty} p^{n-r} (1+p)^r k_s^2 = \lim_{n\to\infty} [p^{1-(r/n)} (1+p)^{r/n}]^n k_s^2.$$

Letting $r/n \to 1-p$ as $n \to \infty$,

$$k_p^2 = \lim_{n\to\infty} [p^p (1+p)^{1-p}]^n k_s^2 \to 0, \tag{3.47}$$

since $p^p (1+p)^{1-p} < 1$ for $0 < p < 1$. This means that the peak of the energy distribution moves to $k \to 0$ as $n \to \infty$. Hence an inverse cascade and condensation of the spectrum at $k = 0$ can be expected from this model. It is interesting to note that the inverse cascade obtained this way is a consequence of the conservation of energy and enstrophy throughout the decay processes, and not of the (selective) dissipation of enstrophy; it originates from the particular property of the matrix element $\Lambda^{k_i}_{k_j k_k}$ in Eq. (3.19) following from Eq. (2.16), and is not the consequence of dissipation.

IV. DYNAMICS OF DRIFT WAVE–ROSSBY WAVE TURBULENCE

As discussed in the Introduction the presence of the dispersive waves in the CHM equation (2.16) gives rise to regimes of wave turbulence that may be analyzed within the context of the weak turbulence and the renormalized turbulence (RNT) wave kinetic equations. In regimes where the statistics of the wave field ϕ are sufficiently random to allow the quasi-Gaussian (or quasinormal) truncation of the multifield correlation functions to be valid, the wave kinetic equation provides an analytical method of describing the distribution of the turbulent fluctuation energy spectrum $W(\mathbf{k}) = (1 + k_\perp^2 \rho_s^2) |\phi_\mathbf{k}|^2$ in wave-number space.

A. Weak turbulence Kolmogorov-like spectral laws

The wave kinetic equation provides a method of deriving Kolmogorov-type spectra by methods developed by Zakharov (1984) and his collaborators. The analysis shows

clearly how the Kolmogorov spectra depend on the scale invariance of both the dispersion law $\omega_{\mathbf{k}}$ and the wave interaction dynamics $\Lambda^{k_1}_{k_2k_3}$. Thus for drift wave–Rossby wave turbulence the spectral distribution changes slope between the long wave region $k_\perp\rho<1$ and the short wave region $k_\perp\rho>1$ where the scaling properties change. In addition, the dispersion law $\omega_{\mathbf{k}}=k_y v_d/(1+k_\perp^2\rho^2)$ is clearly anisotropic, and thus the spectral distributions are of the form

$$W(\mathbf{k})=P^{1/2}\frac{1}{|k_x|^{\nu_x}|k_y|^{\nu_y}} \tag{4.1}$$

with separate scaling exponents $\nu=(\nu_x,\ \nu_y)$ in the two directions. Here P is the flux of the energy in the inertial range. In the long wave region ($k\rho<1$) the analyses of Novakovskii *et al.* (1988), Balk and Nazarenko (1990), and Balk *et al.* (1990,1991) give $\nu_x=3$ and $\nu_y=3/2$, which was tested in numerical simulations by Horton *et al.* (1991). To test the analytic inertial range model an idealized isotropic source–sink model $\gamma^I(k)\phi_{\mathbf{k}}$ is added to the **k**-space CHM equation (3.19). The actual plasma fluctuation source–sink physics occurs through the mechanism of dissipation either in the form of finite resistivity from electron–ion collisions or resonant wave particle interactions. The dynamical description then requires changing the structure of the CHM equation as given in Sec. IV E.

B. Wave-kinetic equation

Here we review the key elements of this rather technically complex field of study. The principal assumption in the analysis is that the energy-momentum transfer within the turbulent spectrum $W(\mathbf{k})$ occurs along the three-wave resonant manifold defined by

$$\begin{aligned}&\mathbf{k}=\mathbf{k}_1+\mathbf{k}_2,\\ &\omega_{\mathbf{k}}=\omega_{\mathbf{k}_1}+\omega_{\mathbf{k}_2},\end{aligned} \tag{4.2}$$

in the $\mathbf{k}\omega$ space. The resonance conditions (4.2) allow both a local(as in the Kolmogorov hypothesis) and nonlocal interaction. In renormalized turbulence theory the sharp delta function condition $\delta(\omega_{\mathbf{k}}-\omega_{\mathbf{k}_1}-\omega_{\mathbf{k}_2})$ on the frequency resonance in condition (4.2) is replaced by a broadened nonlinear propagator $g_{\mathbf{k}\omega}$ with finite correlation time $\tau_c=1/\nu_k$ that is determined self-consistently with the fluctuation spectrum $W(\mathbf{k})$. Taking $\nu_{\mathbf{k}}$ into account is important for determining the spectral linewidths $\Delta\omega$ observed in the electromagnetic scattering experiments discussed in the Introduction. The nonlinear broadening of the propagator $g_{\mathbf{k}\omega}$, however, is not considered to be important in determining the ω-integrated distribution $W(\mathbf{k})=\int d\omega\ W(\mathbf{k},\omega)$ of the fluctuation energy in **k** space.

The transport of fluctuation energy in **k** space occurs resonantly along the three-wave manifold (4.2) which is given in more detail by letting $\mathbf{p}=\mathbf{k}_1$ and $\mathbf{k}_2=\mathbf{k}-\mathbf{p}$,

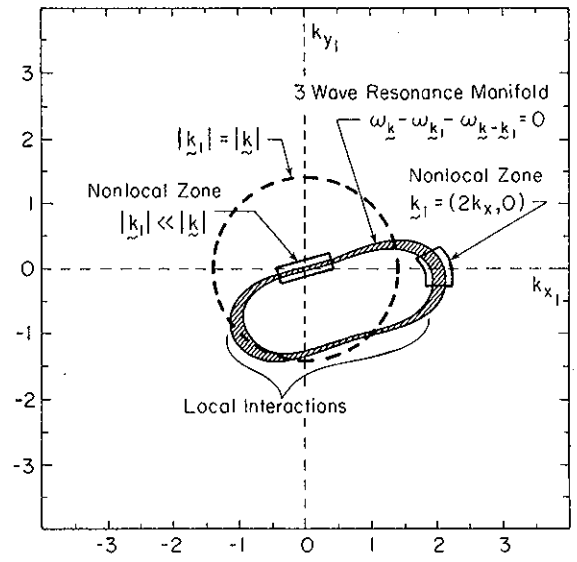

FIG. 3. Resonant three-wave manifold for the drift wave–Rossby wave dispersion relation. For fixed **k**, the zero level contour gives the values of $\mathbf{k}_1$ for which the frequency resonant $\omega_{\mathbf{k}}-\omega_{\mathbf{k}_1}-\omega_{\mathbf{k}-\mathbf{k}_1}=0$ is exactly satisfied. The dashed circle is of radius $|\mathbf{k}|$ so the intersection with resonance manifold gives the region of local interaction. The two special regions of nonlocal interactions are also marked.

$$\Delta\Omega_{\mathbf{k},\mathbf{p}}=\frac{p_y v_d}{1+p_x^2+p_y^2}+\frac{(k_y-p_y)v_d}{1+(k_x-p_x)^2+(k_y-p_y)^2}-\frac{k_y v_d}{1+k_x^2+k_y^2}=0, \tag{4.3}$$

where for each (k_x,k_y) there is a resonant curve in $\mathbf{p}=\mathbf{k}_1$ shown in Fig. 3. The interactions are defined as local in **k** space when all three-wave vectors are comparable in size $|\mathbf{k}|\sim|\mathbf{k}_1|\sim|\mathbf{k}-\mathbf{k}_1|$ It is the interaction of these comparable size fluctuations that is used in the Kolmogorov picture of the inertial range cascade. For example, from the drift wave dispersion relation (3.20) it is easy to see that all equilateral triangles with sides $\mathbf{k}_1$, $\mathbf{k}_2$, $\mathbf{k}=-\mathbf{k}_3$ satisfy the resonant condition $\omega_1+\omega_2+\omega_3=0$ and thus from part of the local transport in **k** space. In addition, there are *nonlocal* transport processes in which one of the **k** vectors is much smaller than the other two. The fluctuation at small $|\mathbf{k}|$ is then part of the large-scale turbulent flow and this large-scale flow can have a dominant influence over the small-scale turbulence. One method of analyzing the nonlocal fluctuation dynamics is by separating the fluctuation field into $\phi=\phi_L+\phi_s$ where L and s are the large-scale and small-scale parts of the field, respectively. The turbulence analysis based on this two-scale analysis is discussed in Sec. V H.

In the three-wave resonant manifold (a three-dimensional surface in the four-dimensional vector space of $\mathbf{k},\mathbf{k}_1=\mathbf{p}$) shown in Fig. 3 there are two important regions of nonlocal contributions to the **k**-space transport processes. The region around the origin defined by $|\mathbf{p}|\ll|\mathbf{k}|$ is one in which **k** and $\mathbf{k}-\mathbf{p}$ are strongly coupled by the large-scale fluctuation **p**. Balk *et al.* (1991) show that these small $|\mathbf{p}|$ interactions reduce to a diffusion of $W(\mathbf{k})$ in **k** space along a

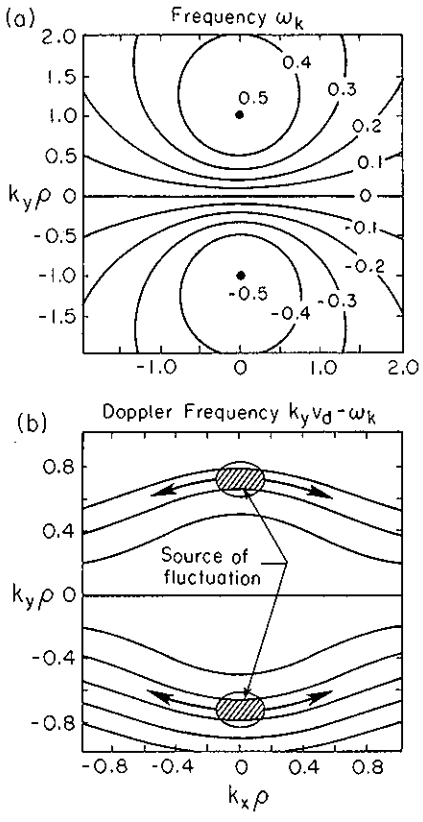

FIG. 4. Isolines of the wave frequency (a) in the center of mass frame and (b) in the frame moving with the drift-Rossby speed $v_d=v_R$.

curve of given $\nu_{\mathbf{k}}=k_y v_d-\omega_{\mathbf{k}}$ as shown in Fig. 4. Such transport takes energy from the source at $k_x\rho=0$, $k_y\rho\sim 0.5$ region of max $\gamma_{\mathbf{k}}$ to the regime of $k_y\rho\to 0$ and finite $k_x\rho$ which is the region of shear flows or zonal flows where $v_y(x,t)\cong -cE_x/B\gg v_x$.

A second region of strong, nonlocal transport occurs from the region around $\mathbf{p}=(2k_x,0)$ as indicated in Fig. 3. In this region the spectral equation contains finite difference terms that directly couple energy from $\mathbf{k}$ to $O(\pm k_x,k_y)$ through the strength of the short-scale shear flow at $(2k_x,0)$. Thus, the combination of the nonlocal and local transport in $\mathbf{k}$ space of fluctuation energy and momentum contained in the turbulent fluctuations is a complex anisotropic process for the CHM equation.

To formulate the transport analysis in $\mathbf{k}$ space under the resonance condition (4.2) and to derive the weak-turbulence Kolmogorov scaling exponents it is necessary to transform the mode coupling Eqs. (3.19) to a form showing the symmetry of the exchange of any two of the three waves $\{k_i,\omega_{k_i}\}_{i=1}^3$ where $\mathbf{k}_3=-\mathbf{k}$, $\omega_3=-\omega_{\mathbf{k}}=\omega_{\mathbf{k}_3}$ and $\Sigma_{i=1}^3\mathbf{k}_i=\Sigma_{i=1}^3\omega_i=0$. The transformation of $\phi_{\mathbf{k}_i}(t)$ to $a_{\mathbf{k}_i}(t)$ required to show the wave exchange symmetry follows naturally from the Hamiltonian formulation of the wave dynamics with $i\dot{a}_j=\delta H/\delta a_j^*$ where the field Hamiltonian is expanded in powers of $a_{k_j}(t)$ with

$$H=\sum_j \omega_{k_j}a_j^*a_j+\frac{1}{3!}\sum_{i,j,k} V_{ijk}a_ia_ja_k\delta_{\mathbf{k}_i+\mathbf{k}_j+\mathbf{k}_k0}+\cdots \tag{4.4}$$

[Balk *et al.* (1990), Appendix A]. The result of the Hamiltonian analysis is that the usual prescription of introducing the plasma number spectrum by $n_{\mathbf{k}}=W_{\mathbf{k}}/|\omega_{\mathbf{k}}|=a_{\mathbf{k}}^*a_{\mathbf{k}}$ and thus $a_{\mathbf{k}}(t)=(1+k^2)\phi_{\mathbf{k}}(t)/|k_y|^{1/2}$ gives the desired symmetric interaction elements. We note that $n_{\mathbf{k}}$ reduces to $N_{\mathbf{k}_p}=N_p$ in Eq. (3.35) at the limit of weak interactions where the linear dispersion relation holds.

It is straightforward to show that the mode coupling elements $\Lambda^{\mathbf{k}}_{\mathbf{k}_1\mathbf{k}_2}$ of Eq. (3.19) are transformed to the fully symmetric $V_{kk_1k_2}$ for the $a_k(t)$ dynamics by

$$V_{-k_3k_1,k_2}=\left|\frac{k_{1y}k_{2y}}{k_{3y}}\right|^{1/2}\frac{(1+k^2)\,\Lambda^k_{k_1,k_2}}{(1+k_1^2)\,(1+k_2^2)}$$
$$=|k_{1y}k_{2y}k_{3y}|^{1/2}\left(\frac{k_{x1}}{1+k_1^2}+\frac{k_{x2}}{1+k_2^2}+\frac{k_{x3}}{1+k_3^2}\right) \tag{4.5}$$

which has complete symmetry in the interchange of any two of the three waves. In making the reduction shown in Eq. (4.5) the resonance condition (4.2) must be used.

Now for sufficiently short wave interaction times the dispersion of the wave frequencies $\omega_{\mathbf{k}}$ over the spectrum of $W(\mathbf{k},t)=|\omega_{\mathbf{k}}|n_{\mathbf{k}}(t)$ allows the fluctuation dynamics to be described by the classical wave kinetic equation [Sagdeev and Galeev (1968)]

$$\frac{dn_{\mathbf{k}}}{dt}=4\pi\int d\mathbf{k}_1d\mathbf{k}_3|V_{\mathbf{k}\mathbf{k}_1\mathbf{k}_2}|^2\delta(\mathbf{k}-\mathbf{k}_1-\mathbf{k}_2)\,\delta(\omega_{\mathbf{k}}-\omega_{\mathbf{k}_1}-\omega_{\mathbf{k}_2})$$
$$\times[n_{\mathbf{k}_1}n_{\mathbf{k}_2}-n_{\mathbf{k}}n_{\mathbf{k}_1}sg(\omega_{\mathbf{k}}\omega_{\mathbf{k}_2})-n_{\mathbf{k}}n_{\mathbf{k}_2}sg(\omega_{\mathbf{k}}\omega_{\mathbf{k}_1})]. \tag{4.6}$$

The kinetic equation (4.6) gives the time rate of change of any functional F with flux $f_{\mathbf{k}}$ defined by

$$F(t)=\frac{1}{2}\int f_{\mathbf{k}}sg(\omega_{\mathbf{k}})n_{\mathbf{k}}(t)d\mathbf{k} \tag{4.7}$$

as

$$\frac{dF}{dt}=2\pi\int |V_{\mathbf{k}\mathbf{k}_1\mathbf{k}_2}|^2\delta(\mathbf{k}-\mathbf{k}_1-\mathbf{k}_2)\,\delta(\omega_{\mathbf{k}}-\omega_{\mathbf{k}_1}-\omega_{\mathbf{k}_2})$$
$$\times n_{\mathbf{k}}n_{\mathbf{k}_1}n_{\mathbf{k}_2}(f_{\mathbf{k}}-f_{\mathbf{k}_1}-f_{\mathbf{k}_2})$$
$$\times\left(\frac{sg(\omega_{\mathbf{k}})}{n_{\mathbf{k}}}-\frac{sg(\omega_{\mathbf{k}_1})}{n_{\mathbf{k}_1}}-\frac{sg(\omega_{\mathbf{k}_2})}{n_{\mathbf{k}_2}}\right)d\mathbf{k}\,d\mathbf{k}_1\,d\mathbf{k}_2. \tag{4.8}$$

Thus any flux $f_{\mathbf{k}}$ which is conserved,

$$f_{\mathbf{k}}=f_{\mathbf{k}_1}+f_{\mathbf{k}_2}, \tag{4.9}$$

under the resonant interactions defined by Eq. (4.2), gives an integral of the motion through Eq. (4.8) with $dF/dt\equiv 0$. Thus, from the resonance conditions (4.2) themselves the total energy-momentum conservation laws for

$$W=\int W(\mathbf{k})d\mathbf{k}\equiv\frac{1}{2}\int |\omega_{\mathbf{k}}|n(\mathbf{k})d\mathbf{k}, \tag{4.10}$$

$$P_x=\int k_x n(\mathbf{k})sg(\omega_k)d\mathbf{k}, \tag{4.11}$$

$$P_y=\int k_y n(\mathbf{k})sg(\omega_k)d\mathbf{k}, \tag{4.12}$$

immediately follow. The conserved P_y momentum is equivalent to the enstrophy conservation using $k_y n_{\mathbf{k}} sg(\omega_{\mathbf{k}}) = (1+k^2)^2|\phi_k|^2$ so that $P_y = W+U$ is defined as in Eqs. (3.1) and (3.2). The momentum $P_x=0$ for a symmetric or antisymmetric wave field $\phi(-x,y,t)=\pm\phi(x,y,t)$ which reduces the invariants to W and U. In general, the broken symmetry in x of the actual physical equilibrium leads to $P_x\neq 0$, and the conservation of P_x gives a constraint on the radial transport.

The existence of an additional invariant in the weak turbulence equation has been shown by Zakharov and his collaborators to be a signature of the integrability that occurs in the original nonlinear PDEs, as shown in studies of the Korteweg–de Vries, Kadomtsev–Petviashvili, and nonlinear Schrödinger equations [Zakharov and Schulman (1988)]. For the CHM equation Balk *et al.* (1991) show that there is a remnant of the integrability by finding an additional invariant of Eq. (4.6) given by $f_{\mathbf{k}}=\omega_{\mathbf{k}}^3/k_x^2$. The implication of this additional invariant F is shown to be connected with the nonlocal interactions that generate a flux of energy along the curves of constant $\nu_{\mathbf{k}}=k_y v_d-\omega_{\mathbf{k}}$ shown in Fig. 4. The invariant of P_y, W, and F (associated with $\omega_{\mathbf{k}}^3/k_x^2$) restrict the directions of the fluxes of these conserved quantities and the regions of energy dissipation. Zakharov and collaborators show that the fastest transport in $\mathbf{k}$ space is the nonlocal transport from the region of $|\mathbf{p}|\ll|\mathbf{k}|$ in Fig. 3 where the large-scale ($|\mathbf{p}|\ll 1$) fluctuations $n(\mathbf{p})$ produce a flux of energy from ($k_x=0$, $k_y\rho_s\sim 1$) to $|k_x|\gg k_y|$ along the curves of constant

$$\nu_{\mathbf{k}}=k_y v_d-\omega_{\mathbf{k}}=\frac{k_y v_d(k_x^2+k_y^2)}{1+k_x^2+k_y^2} \tag{4.13}$$

shown in Fig. 4(b).

The transport of fluctuation energy along the curves of constant $\nu_{\mathbf{k}}$ leads directly to the buildup of strong, small-scale zonal flows with $|k_x|\gg|k_y|$. The fluctuation spectrum $W(k_x,|k_y|\ll 1)$ has a steep power lower drop-off $1/|k_x|^{\nu_x}$ with $\nu_x\geq 2$ for $k_x>1$. We now derive the various Kolmogorov scaling exponents in the two scaling zones of $\mathbf{k}$ space.

C. Scaling laws

The dynamics of the turbulent interactions is known from simulations and theory to have different strengths in the long wave $k\ll 1$ and short wave $k\gg 1$ regions. The scaling properties for these two regions follow from the scaling laws for the dispersion and interaction elements for the waves,

$$\omega_{qk}=q^{\alpha}\omega_k, \quad V_{qk,qk_1,qk_2}=q^{\beta}V_{k,k_1k_2}, \tag{4.14}$$

where q is the scaling factor for the wave number $k\to qk$ and $\alpha=(\alpha_x,\alpha_y)$ and $\beta=(\beta_x,\beta_y)$ are the scaling exponents. From (3.20) and (4.5) we see that for the short waves $\alpha=(-2,1)$ and $\beta=(-1,3/2)$ whereas for long waves $\alpha=(2,1)$ and $\beta=(3,3/2)$. (For long waves the relevant dispersion law for scaling is for $\nu_k=\omega_k-k_y v_d$ rather than ω_k.) Using the scaling analysis of Zakharov as applied to drift-Rossby waves by Novakovskii *et al.* (1988), Mikhailovskii *et al.* (1988), and Balk *et al.* (1990,1991) we obtain the following wave-number distributions:

$$W(k_x,k_y)=\begin{cases} W_0\left(\frac{k_0}{k_x}\right)^2\left(\frac{k_0}{k_y}\right)^{3/2}, & k_x\rho_s\gg 1, \\ W_0\left(\frac{k_0}{k_x}\right)^3\left(\frac{k_0}{k_y}\right)^{3/2}, & k\rho_s\ll 1. \end{cases} \tag{4.15}$$

These scaling laws are required for $dn(\mathbf{k})/dt=0$ in the inertial range of $\mathbf{k}$ where $\gamma(\mathbf{k})=0$.

If we consider the omnidirectional k scaling in Eqs. (4.15) the two scaling law regimes are $W(k)=W_0(k_0/k)^{7/2}$ and $W_0(k_0/k)^{9/2}$ where the exponents 7/2 and 9/2 bracket the scaling exponent of 4 reported by Hasegawa *et al.* (1978). An exponent of 4 leads to the omnidirectional spectral density $\int dk\, kW(k)=\int dk\, W_0(k_0/k)^3$ of 3. The exponent of 3 is commonly used in practical estimates of transport and appears consistent with the electromagnetic scattering measurements.

Numerical simulations by Terry and Horton (1982, 1983); Waltz (1983, 1990), and Horton (1986) have shown anisotropic spectra for the CHM equation, but have not been constructed to have an inertial range. The simulation of Horton *et al.* (1991) is constructed to have an inertial range, and the scaling exponents are reported as briefly discussed in the next subsection.

The energy spectrum (3.4) corresponds to the local thermodynamic equilibrium $n(\mathbf{k})=T/(|\omega_{\mathbf{k}}|+|k_y|v)$ corresponding to the Rayleigh–Jeans law for the system. Here T and v are constants. This thermodynamic equipartition solution does not have a finite energy-momentum flux in $\mathbf{k}$ space. The finite energy-momentum flux through the inertial range is given by the Kolmogorov-type spectra (3.44) and (4.15). Thus the driven-damped system must develop spectra of the Kolmogorov type in the inertial range as we now illustrate with numerical simulations.

D. Inertial range simulation

A test of the scaling exponents and the shape of the driven-damped CHM equation was carried out by Horton, Su, and Morrison (1991). In these tests the CHM equation is solved in a truncated $\mathbf{k}$ space as written in Eq. (3.18) using the mode coupling elements $\Lambda^{\mathbf{k}}_{\mathbf{k}_1,\mathbf{k}_2}$ in Eq. (3.19). To study the inertial range the source–sink term $\gamma_{\mathbf{k}}\phi_{\mathbf{k}}(t)$ is added to the right-hand side by $\omega_{\mathbf{k}}\to\omega_{\mathbf{k}}+i\gamma_{\mathbf{k}}$ with the choice

$$\gamma\mathbf{k}=\begin{cases} \gamma_0=+0.005, & \text{for } 0.35\leq|\mathbf{k}|\leq 0.4, \\ 0, & \text{for } 0.4<|\mathbf{k}|<2.0, \\ -\gamma_0=-0.005, & \text{for } |\mathbf{k}|>2.0. \end{cases} \tag{4.16}$$

Computations were carried out on the grid with $\mathbf{k}=(m,n)k_1$ with $k_1\rho=0.05$ giving the periodic box size of $(128\rho)^2$ for times up to $t_{\max}=1000$. Contour plots of the potential field $\phi(x,y,t=700)$ are given in Fig. 5. The simulation mode energy spectra in the steady state are peaked at $k\rho=0.35$

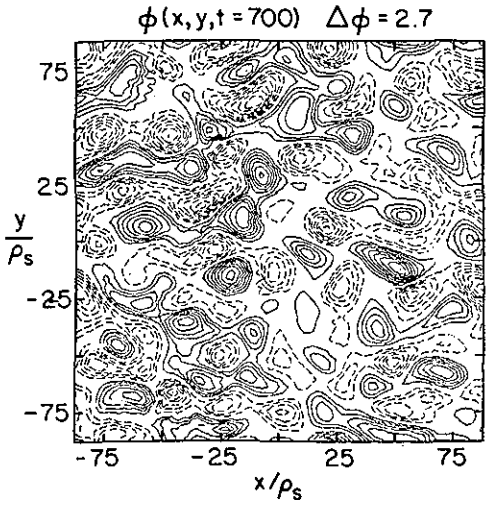

FIG. 5. Contours of the potential/streamfunction for the driven-damped CHM equation constructed to test the inertial range scaling exponents.

(the source region) and decay in the inertial range as shown in Fig. 6. Parametrizing the numerically computed one-dimensional projections to

$$W^{\mathrm{num}}(k_x)=\sum_{k_y} W(k_x,k_y)\leftrightarrow\frac{1}{|k_x|^{m_x}},$$
$$W^{\mathrm{num}}(k_y)=\sum_{k_x} W(k_x,k_y)\leftrightarrow\frac{1}{|k_y|^{m_y}}, \tag{4.17}$$

the regression fits to the simulation data determine the values of $m_x\pm\delta m_x$ and $m_y\pm\delta m_y$.

The simulations show the change in the indices m_x, m_y in the high (m^h) and low (m^l) wave-number regimes as expected from the scaling theory Eq. (4.15). The exponents found in the example given in Eq. (4.16) shown in Fig. 6 are

$$m_x^h=1.6\pm0.1,\quad m_y^h=1.6\pm0.1,\quad \text{for}\quad k>1,$$
$$m_x^l=3.7\pm0.4,\quad m_y^l=4.1\pm0.4,\quad \text{for}\quad k<1, \tag{4.18}$$

which confirms the trend but not the values of the scaling laws based on the asymptotic forms of Eq. (4.15). The steeper decrease of the numerical k_xk_y spectrum is either due to the compressed inertial range used in the test or due to the asymptotic theoretical reductions of $1+k^2\to1$ and k_x^2 used in obtaining the α and β scaling exponents from the ω_k and $V_{kk_1k_2}$ formulas.

In the steady state shown in Figs. 5 and 6 the total turbulent energy density and enstrophy are $W=0.8$ and $U=0.3$ in units of $(\rho/L_n)^2n_0T_e$. The space–time-averaged kurtosis and skewness of ϕ are 2.9 and -0.1, respectively. The system appears to be within the state of weak turbulence for these small values of γ_0.

A closely related simulation of drift wave turbulence driven by the parallel velocity ($\gamma_{\max}\simeq|du_\parallel/dx|$) shear flow in the ion-acoustic wave equation gives the spectra indices $m_x=2$ for $0.2<k_x\rho<2$ and $m_x\cong3$ for $2<k_x\rho<7$ [Horton

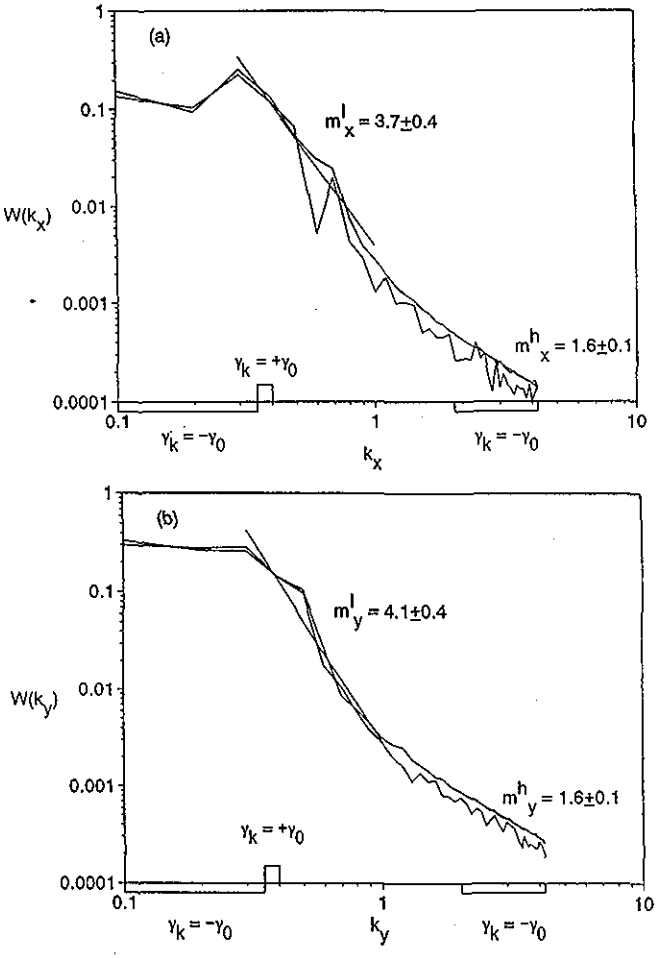

FIG. 6. The-one dimensional energy spectra $W(k_x)$ and $W(k_y)$ for the driven-damped system with fittings for the inertial range exponents. The profile of the source–sink term is shown along the k axis. The smooth curve is the time-averaged spectrum while the bumpy curve is the instantaneous spectrum.

et al. (1993)]. Huld *et al.* (1991) show vortices and vortex transport produced by the KH instability in the edge of low temperature-density plasma.

Even in the isotropic, 2-D Euler limit given by Eq. (2.17) the question of the value of spectral index remains an active area of research. High resolution simulations of the forced-damped 2-D Euler equation persistently show energy spectral decays faster than the rate $k^{-3}[\ln(k/k_1)]^{-1/3}$ predicted by space filling, isotropic, homogeneous turbulence theory. The reason for the large decay indices has been traced to the emergence of long-lived, coherent vortex structures [McWilliams (1984) and Legras *et al.* (1988)]. The high resolution simulations of Legras *et al.* (1988) show clearly the correlation of larger decay indices ($m\simeq4$) with the appearance of monopole, dipole, and tripolar vortices. Legras *et al.* (1988) compare the spectral indices and the associated vortex structures for $(512)^2$ simulations obtained with the three types of drivers (i) constant, single mode $\mathbf{k}=(k_l,0)$, forcing; (ii) stochastic, narrow-band external forcing $\tilde{F}(k_1<|\mathbf{k}|<k_2)$ taken with new random phases at each time step; and (iii) narrow-band linear growth rate similar to that given in Eq. (4.16). A large-scale damping rate $-\nu_L\phi(\mathbf{k})$ and

a hyperviscosity $-\nu_s(k_\perp^2)^p\phi(\mathbf{k})$ are used to produce the steady state. The resulting turbulence is characterized by the spectral index m and its vortex content as follows: (i) $m=3.6$ and a low-packing fraction of relatively large vortices; (ii) $m=3.5$ and a denser packing of smaller vortices; and (iii) $m=4.2$ and the prominence of several dipolar and one tripolar vortex. Thus, it appears that for 2-D turbulence the space filling, inverse cascade spectrum of $k^{-3}[\ln(k/k_1)]^{-1/3}$ is an idealization that is not achieved in practice due to the strong, self-organization properties of these turbulent flows. A further demonstration of the suppression of turbulent cascades by coherent vortices in 2-D turbulence is given by McWilliams (1990a, 1990b).

In contrast, in the next subsection we consider the case where self-consistent wave growth and damping due to electron–ion collisions are used to drive the system. For typical values of these parameters the system enters a state of strong turbulence which is a more isotropic state.

E. Self-consistent driven-damped nonlinear drift wave equation

Fluctuations in tokamaks with characteristics of the drift waves are widely observed in many confinement experiments since the 1976–1978 electromagnetic scattering experiments described in the Introduction. The exact nature of the driving and damping mechanisms has proven difficult to determine experimentally [Bravenec *et al.* (1992)] and presumably varies widely with the confinement system parameters, the plasma parameters, and plasma profiles as linear stability theory predicts. The simplest and earliest form of driving and damping of the drift wave fluctuations occurs through the electron–ion collisions that determine the plasma resistivity $\eta=m_e\nu_{ei}/n_e e^2$ and the ion–ion collisions that determine the plasma viscosity $\mu_\perp=0.3\nu_{ii}\rho_i^4$ and $\mu_\parallel=(T_i/m_i\nu_{ii})$. For fluctuations with wave numbers $k_\perp$, $k_\parallel$ perpendicular to and parallel to the magnetic field the associated decay rates are

$$\begin{aligned}\nu_\parallel^\eta&=\frac{k_\parallel^2 T_e}{\eta e^2 n_e}=k_\parallel^2 v_e^2/\nu_{ei}\ll|k_\parallel|v_e,\\ \nu_\perp^\mu&=k_\perp^4\mu_\perp=0.3k_\perp^4\rho_i^4\nu_i\ll\nu_i,\\ \nu_\parallel^\mu&=k_\parallel^2 v_i^2/\nu_i\ll|k_\parallel|v_i.\end{aligned}\tag{4.19}$$

It is well known that the resistive diffusion $\nu_\parallel^\eta$ is destabilizing and the viscous dampings $(\nu_\perp^\mu,\nu_\parallel^\mu)$ are stabilizing. In the limit of low collision frequency the dissipation is replaced with the collisionless Landau damping which is adequately described by the limiting formulas $\nu_\parallel^\eta\to|k_\parallel|v_e$ and $\nu_\parallel^\mu\to|k_\parallel|v_i$ and $\nu_\perp^\mu\to0$.

There are two well-known descriptions of the resistive-dissipative drift wave turbulence: (1) the Horton $i\delta_k$ model (1976, 1986) that retains the single field description but introduces an anti-Hermitian operator $\hat{\mathcal{L}}^{ah}\phi$ to include the effects of the dissipation, and (2) the Hasegawa–Wakatani (1983) model that introduces two fields, the density and the electrostatic potential to describe the dissipative dynamics and the partial decoupling of the density and potential that occurs when the dissipation is strong. For weak dissipation the Hasegawa–Wakatani equation reduces to the $i\delta_k$ model [Horton (1986)]. Finally, a more complete collisional description that includes the coupling to the ion-acoustic waves and the electron temperature fluctuations $(\tilde\phi,\tilde n,\tilde u_\parallel,\tilde T_e)$ is given by Hinton and Horton (1971) in a work on the interpretation of the collisional drift wave experiments. The drift wave measurements analyzed were those of Hendel *et al.* (1968) in a long, straight cylindrical geometry containing a thermionically ionized cesium plasma, a device called a Q-machine for the quiescent plasma produced. The four-field system $(\tilde\phi,\tilde n,\tilde u_\parallel,\tilde T_e)$ and other reduced equation drift wave models are analyzed in Horton (1990) and in more detail in Scott (1992). Here we restrict the discussion to the Horton $i\delta_k$ model and the Hasegawa–Wakatani equations.

In the limit of weak dissipation the electron density response to the electrostatic potential is nonlocal and dissipative as given by

$$\tilde n(x,y,t)=\frac{en_0}{T_e}\left(\phi+\delta_0(c_1+\nabla^2)\frac{\partial\phi}{\partial y}\right)=\left(\frac{en_0}{T_e}\right)(1+\hat{\mathcal{L}}^{ah})\phi,\tag{4.20}$$

where the anti-Hermitian operator $\hat{\mathcal{L}}^{ah}$ is of strength δ_0 and in general has the power series expansion $\delta_0(c_1+c_2\nabla^2+c_3\nabla^4+\cdots)\partial y$. With the generalization of the electron density response from that in Eq. (2.5) to that in Eq. (4.20) it is straightforward to repeat the analysis leading to Eq. (2.16) to obtain the dissipative drift wave equation used by Horton and his collaborators,

$$\hat{\mathcal{L}}\frac{\partial\phi}{\partial t}+v_d\frac{\partial\phi}{\partial y}+\left(\frac{\partial\phi}{\partial x}\frac{\partial}{\partial y}(\hat{\mathcal{L}}\phi)-\frac{\partial\phi}{\partial y}\frac{\partial}{\partial x}(\hat{\mathcal{L}}\phi)\right)+\mu\nabla^4\phi=0,\tag{4.21}$$

where

$$\hat{\mathcal{L}}=1-\nabla^2+\hat{\mathcal{L}}^{ah},\tag{4.22}$$

and μ is the perpendicular ion viscosity that arises from the divergence of the ion cross-field current,

$$\mathbf{j}_\perp=\left(\frac{c\mathbf{B}}{B^2}\right)\times\left[m_i n_i\left(\frac{d\mathbf{v}_\perp}{dt}\right)-\mu_\perp\nabla^2\mathbf{v}_\perp\right],$$

with $\mathbf{v}_\perp=c\mathbf{E}\times\mathbf{B}/B^2=c\hat{\mathbf{z}}\times\nabla\phi/B$. The model equation is also called the $\mathbf{E}\times\mathbf{B}$ nonlinear drift wave model since the nonlinearity of the Poisson bracket now contains both the polarization drift $[\phi,\nabla^2\phi]$ nonlinearity and the nonlinearity due to the $\mathbf{E}\times\mathbf{B}$ convection of the density

$$\mathbf{v}_E\cdot\nabla n=[\phi,n]=[\phi,\hat{\mathcal{L}}^{ah}\phi].\tag{4.23}$$

Waltz (1983, 1990) has compared the contributions of the two nonlinearities and shown from simulations that the $\mathbf{E}\times\mathbf{B}$ nonlinearity is essential for saturation at the mixing length level. Without the $\mathbf{E}\times\mathbf{B}$ nonlinearity the RMS amplitude of the fluctuations continues to increase with δ_0 beyond the mixing length (ml) level given by

$$\frac{\tilde n^{ml}}{n}\sim\frac{e\tilde\phi^{ml}}{T_e}\sim\frac{\lambda_x}{n_0}\frac{dn_0}{dx}.\tag{4.24}$$

The linear modes for the dissipative equation are given by

$$\omega_{\mathbf{k}}+i\gamma_{\mathbf{k}}=\frac{k_y v_d - i\mu_\perp k_\perp^4}{1+k_\perp^2+i\delta_0 k_y(c_1-k_\perp^2)}, \tag{4.25}$$

with γ_k being positive in the region of $k\rho<1$ with $\gamma_{\mathbf{k}}' \simeq k_y^2\delta_0(k_\perp^2 - c_1)/(1 + k_\perp^2)^2$ and negative in the short wave region $k\rho>1$ with $\gamma_{\mathbf{k}}\simeq-\mu_\perp k_\perp^4/(1 + k_\perp^2)$. A typical distribution of $\gamma(k_x,k_y)$ is shown in Fig. 7.

The relationship between the "mixing length" description of turbulence and the "direct interaction approximation" and RNT turbulence theories is analyzed by Sudan and Pfirsch (1992).

The dissipative nonlinear drift wave equation shows both regimes of weak turbulence with $W=\Sigma_{\mathbf{k}} W(\mathbf{k})\ll 1$ and strong turbulence $W\gg 1$ where the vortex gasdynamics dominates. An example of the vortex gas regime is shown in Fig. 8 where the parameter set is $\{\delta_0,c_1,\mu\}$ $=\{1/4,-1/4,0.005\}$, taken to be representative of the trapped electron turbulence in tokamaks, is used. The total energy and enstrophy in the saturated state is $W=25.6$ and $U=2.1$, which gives a mean wave number of $\bar{k}\rho_s=(U/W)^{1/2}=0.28$. The dimensionless dissipative Reynolds number for the system is

$$R_{en}=\frac{\tilde{v}_E L}{\mu}=2\times 10^3, \tag{4.26}$$

where $L=62.8\rho_s$. The dissipationless Reynolds number or Kubo number formed by the ratio of the convective derivative nonlinearity and the wave frequency $\omega_{\bar{k}}$ is

$$R_E=\frac{\bar{k}\tilde{v}_E}{\omega_{\bar{k}}}\sim 2, \tag{4.27}$$

a value of R_E characteristic of drift wave vortices with speeds close to the drift wave speed. Having $R_E>1$ puts the drift wave dynamics in the regime of self-trapping of the wave energy into vortices. This regime of self-trapping significantly reduces the effect of inhomogeneities on the waves, as shown in Sec. V G, and greatly increases the lifetime of the fluctuation.

The condition for self-trapping is just above the mixing length level as shown, noting that a circular vortex of radius r_0 has an effective wave number $\bar{k}r_0\simeq\pi$ and thus using $\omega_{\bar{k}}/k_y\cong v_d$ and $\tilde{v}_E=\bar{k}c\tilde{\phi}/B$ we obtain from Eq. (4.27)

$$\frac{c\phi_{\max}}{B}>r_0 v_d=\frac{r_0}{L_n}\frac{cT_e}{eB}\frac{2}{\pi} \tag{4.28}$$

which corresponds to an amplitude just above the mixing length level (4.24).

Kono and Miyashita (1988) show an example of drift wave turbulence condensing to a final dipole vortex state.

In the vortex regime (4.28) there is trapped fluid or plasma [Horton and Petviashvili (1993)] that rotates around the potential maximum at the rate Ω_E. We calculate the rotation rate from the local model of vortex with $\phi=\phi_{\max}(1-r^2/r_0^2)$ to obtain angular rotation frequency

$$\Omega_E=\frac{v_\theta}{r}=\frac{c}{rB}\frac{d\phi}{dr}=-\frac{2c\phi_{\max}}{Br_0^2} \tag{4.29}$$

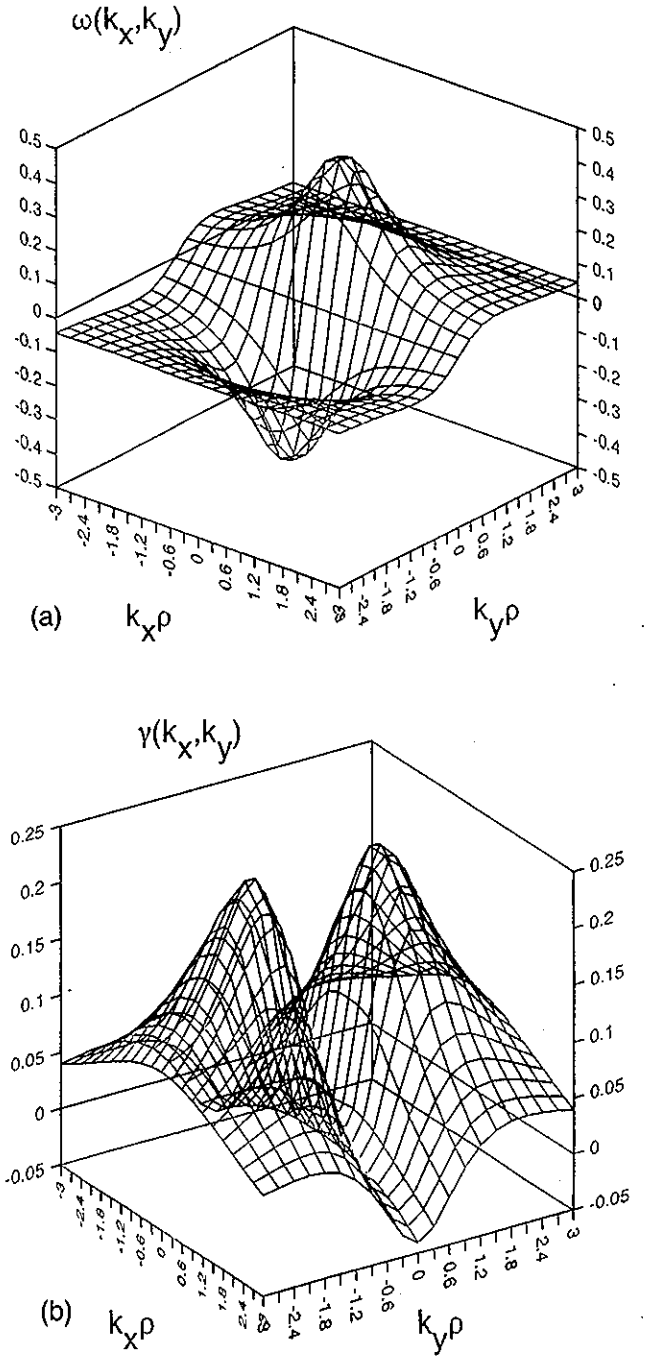

FIG. 7. Perspective plots in the center of mass frame of the wave frequency $\omega(k_x, k_y)$ and the growth-damping rate $\gamma(k_x,k_y)$ for the dissipative drift wave equation (4.21) with (4.25).

which is clockwise for $\phi_{\max}>0$ where the pressure and density are high (anticyclone) and counterclockwise for $\phi_{\max}<0$ where the pressure and density are low.

Thus, the solid curves where $\phi>0$ in Fig. 8 describe the high pressure anticyclones and the dashed curves describe the low pressure cyclones. These vortices are observed in rotating water tank experiments by Nezlin (1986), Antonova *et al.* (1983), Antipov *et al.* (1982), Sommeria *et al.* (1991), and Behringer *et al.* (1991). They are observed to have long lifetimes when $2\pi/\Omega_E$ is small compared to the linear wave

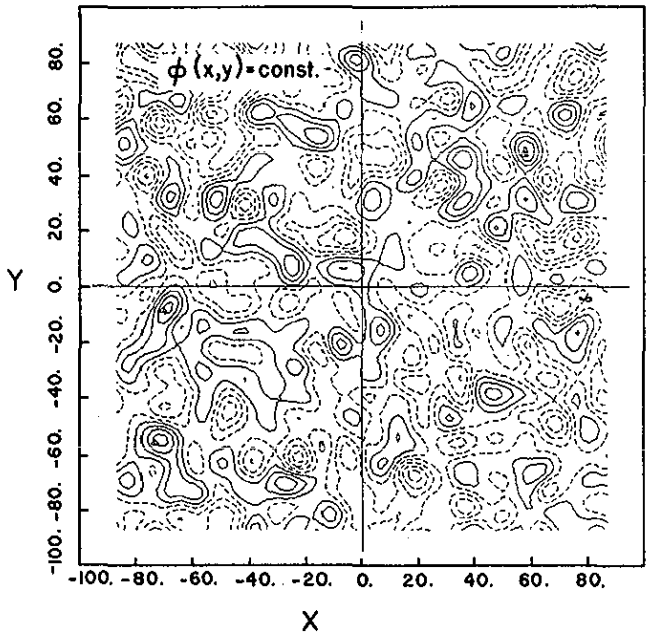

FIG. 8. Contours of equipotential/streamfunction at a given time for a saturated state of strong turbulence from the dissipative drift wave equation with parameters $\phi_0=1/4$, $c_1=1/4$, $\mu=0.005$.

period and the dissipation time scale from the friction of the rotating fluid with the walls of the vessel. Some experiments [Nezlin (1986)] show that the anticyclone has a longer lifetime than the cyclone which is not a property predicted by the dissipative equation (4.21) which has the symmetry $\phi(-x,y,t)=-\phi(x,y,t)$. As we show in Sec. V C for larger scale vortices there is a structural change in the nonlinear equation that brings in the new nonlinearity

$$\alpha\phi\frac{\partial\phi}{\partial y}\equiv\text{scalar or KdV nonlinearity} \tag{4.30}$$

that has the property of removing the degeneracy of the cyclones and anticyclones. Nezlin argues, as supported by theory and simulations, that this nonlinearity is important in the rotating water tank experiments and has the sign of the strength parameter α such that the anticyclonic vortices form the long-lived self-organized structures.

Vortex dynamics has also been observed in the plasmas produced in Q-machines. In the experiments of Pécseli *et al.* (1984, 1985), externally excited vortices of like signs were shown to coalesce into one vortex. Vortices of opposite signs were reported to interact with each other but no claim was made about the formation of a dipole vortex pair. The presence of vortices in a spectrum of waves change the wavenumber spectrum making the spectral decay index m appreciably larger than the values of $m=3$ to 4 derived in Secs. III E and IV C.

V. STABILITY AND DYNAMICS OF THE DRIFT-ROSSBY VORTICES

In this section we review recent developments in the stability of the dipolar vortex solutions and describe the associated vortex wave dynamics of the drift wave–Rossby wave systems.

A. Stability of the dipolar vortex

The numerical simulations of both head-collisions [Flierl *et al.* (1980); Makino *et al.* (1981); McWilliams *et al.* (1981); McWilliams and Zabusky (1984)] and collisions with the impact parameter $b\sim a$ by Horton (1989) show that the dipoles have a high degree of stability and resilience. Efforts to prove stability analytically have failed for the reasons described here.

From simulations and physical reasoning we can see that there are two types of unstable perturbations: (1) the addition of an overall shear flow and (2) the addition of a monopolar structure often called a "rider." The addition of a shear flow gives $\phi\rightarrow\phi_{dp}+\frac{1}{2}(dv_y/dx)x^2$ which produces a stagnation point at $v_y(x,y=0)=d\phi_{dp}/dx+xdv_y/dx=0$. Here $\phi_{dp}(x,y-ut)$ is the dipolar vortex given in Eq. (3.16). For small $v_y'\equiv dv_y/dx$ the stagnation point occurs in the exponentially shielded part of the vortex and the effect is weak. For larger v_y', however, the stagnation point allows the leakage of the trapped potential vorticity to escape from the lobe that is counter-rotating to the vorticity in the shear flow. The leakage allows the decay of the counter-rotating vortex lobe leaving the final state as one with a single monopolar vortex embedded in the shear flow [Horton, Tajima, and Kamimura (1987)].

For the plasma physics problem the presence of a sheared magnetic field also gives a leakage of trapped plasma from the two lobes of the dipole vortex, both lobes in this case, and is described in Sec. V G on wave radiation. For the shear flow we can estimate the condition for a rapid transformation from dipolar to a monopolar vortex from shear flow is that $av_y'\gtrsim u\sim v_d$. We now discuss the effect of adding a symmetric rider $\phi_0(r)$ to the antisymmetric dipole.

The application of a small symmetric rider $\phi\rightarrow\phi_{dp}(r,\theta)+\phi_0(r)$ with a localization radius R comparable to the dipole radius desymmetrizes the dipole giving one side a stronger vorticity. The side with the stronger vorticity then convects the neighboring vortex more strongly and vice versa for the effect of the weaker side on the stronger side. This asymmetry causes the dipole to propagate at a tilted angle with respect to the original $v_d\hat{\mathbf{y}}$ drift direction. Now by considering the conservation of the potential vorticity

$$q(x,y,t)=\nabla^2\phi-\phi+v_dx=\text{constant along fluid trajectory,} \tag{5.1}$$

we can see from $\delta q=0$ that for the resulting displacement δx to have a restoring influence on ϕ in the vortex lobes where $\nabla^2\phi/\phi<0$, we must have the dipole polarization such that $\mathbf{E}_{dp}\times\mathbf{B}$ (or $\hat{\mathbf{z}}\times\nabla\phi_{dp}$) is opposite to the direction of wave propagation ($v_d\hat{\mathbf{y}}$ or $v_R\hat{\mathbf{y}}$). On the other hand, for dipoles oriented such that $\mathbf{E}_{dp}\times\mathbf{B}$ is parallel to the direction of wave propagation there is no restoring tendency from the conser-

vation of q since now the ϕ and $v_d x$ terms are of the same sign. As the angle of deviation increases, one lobe soon dominates over the other.

In the geophysical coordinates the situation is shown in Fig. 9 (Plate 5) where the westward traveling dipole has $a=6\rho_g$ and $u/v_R=1.2$ with $\phi_{\max}\simeq a(u-v_R)\simeq a\,v_R/5$. A small (2%) axisymmetric perturbation $[\phi_0(r)=v_R a/(1+r^2/R^2)]$ is added at $t=0$. The perturbation increases the strength of the northern anticyclone which then swings the weaker southern cyclone to the north. The dipole tilts to about $\pi/2$ and then splits apart. In Fig. 9(b) (Plate 5) at $tv_R/\rho_g=50$ the structure is just coming apart, and by $tv_R/\rho_g=100$ in Fig. 9(c) (Plate 5) there is only the strong anticyclonic monopole with the previous cyclonic part now dispersing as a wave train. This situation of an anticyclone plus a wake of waves continues as shown in Fig. 9(d) (Plate 5) for $tv_R=150\rho_g$.

A single monopolar structure is not an exact solitary wave solution to the CHM equation, but it does form a long-lived structure when the trapping condition is satisfied which is equivalent to the internal rotation frequency $\Omega_E>v_d/r_0$. The monopolar coherent structure can be calculated analytically and is shown to have the shelf (or plateau) shown clearly in Fig. 9(d) (Plate 5) that extends on the northern side of the anticyclone.

B. Lyapunov stability analysis of dipolar vortices

Considerable research effort has been expended to find the mathematically correct stability conditions on the dipolar parameters (u,a) corresponding to the stability behavior observed in the numerical experiments with dipole vortices. At the present time there is no satisfactory derivation of the stability properties of the dipole vortices. The original efforts by Laedke and Spatschek (1986, 1988) have provided the stability theory formulation used by most authors. Rather than search the linear stability equation for the spectrum of unstable eigenmodes $\delta\phi(x,y)e^{st}$ of the dipolar vortex $\phi_{\rm dp}$, the technique is to use Lyapunov stability theory. Laedke and Spatschek and others use the equation governing the perturbation $\delta\phi(x,y,t)$,

$$(1-\nabla^2)\frac{\partial\delta\phi}{\partial t}=\hat{\mathbf{z}}\cdot\nabla(ux+\phi_{\rm dp})\times\nabla(\nabla^2\delta\phi-g\,\delta\phi),\qquad(5.2)$$

where $g=-\lambda^2$ for $r<a$ and $g=\rho^2$ for $r>a$ along with continuity of $\delta\phi$ and $d\delta\phi/dr$ at $r=a$ and $\delta\phi(r\to\infty)\to 0$, to construct the quadratic functional invariant of the motion $L[\delta\phi]$—the Lyapunov functional. That is, $dL/dt=0$ under the motion given by Eq. (5.2) and the boundary conditions that $|\delta\phi|\to 0$ as $r\to\infty$.

In addition, four other invariants of the linear motion $\int(\delta\phi-\nabla^2\delta\phi)[1,x,y,(ux+\phi_{\rm dp})^2]\,dx\,dy$ are used as constraints on the admissible functions $\delta\phi$. The main idea is then to attempt to show that the invariant $L[\delta\phi]$ cannot vanish. Then the Lyapunov argument for stability follows. A similar argument is given by Gordin and Petviashvili (1985) in which a finite, positive definite energy $W(\delta\phi)$ integral invariant and the Casimir invariants chosen to cancel the first-order δW variation about the stationary solution $\phi_{\rm dp}$, are used to derive a second-order $\delta^2 W(\delta\phi)$ stability principle. When $\delta^2 W(\delta\phi)$ is positive definite, the system is stable.

Both groups of authors claim to have proved stability but have failed. The failures of the arguments are explained in mathematical terms by Nycander (1992) and by way of giving a counterexample by Muzyler and Reznik (1992). The counterexample given by Muzyler and Reznik (1992) is a physically realistic perturbation. They are able to show that the perturbation found is such as to make the $L[\delta\phi]$ and $\delta^2 W(\delta\phi)$ integrals negative. The integrals are carried out analytically. They then explicitly study the parameters that make the functionals $L[\delta\phi]$ and $\delta^2 W[\delta\phi]$ negative. The effect of the perturbation used in the counterexample is to give a tilt to the dipole. The counterexample of Muzyler and Reznik is consistent with the tilting instability shown in Fig. 9 from Jovanović and Horton (1993a).

The absence of a general stability theorem of the dipole vortex structures appears consistent with the stability studies of Swaters (1986) and Pierini (1985). Swaters introduces a mean wave number η of the perturbation by using the ratio of enstrophy to energy integrals for the perturbation. The loss of the positive definiteness of the Lyapunov functional is shown to depend on the ratios u/v_d and η/λ where λ is the inner ($r\leqslant a$) wave-number parameter of the mode structure defined in Eq. (3.16). (For the ground state vortex, $3.8<\lambda a<5.2$.) In particular, Swaters asserts that (i) vortices propagating parallel to the waves ($uv_d>0$) lose their stability for long wavelength perturbations ($\eta\ll\lambda$) and (ii) vortices propagating opposite to the waves ($uv_d<0$) lose their stability to short wavelength perturbations ($\eta\gg\lambda$). The first result (i) is consistent with result of Pierini (1985) where vortices with $uv_d>0$ are shown to be stable to small-scale ($\eta\gg\lambda\sim 1/a$) perturbations.

An example of this dependence of stability on direction of propagation is shown in Fig. 10. For a 2% large scale $\eta a\sim 1$ monopolar perturbation the vortex with $uv_d<0$ in Fig. 10(a) is stable whereas the vortex in Fig. 10(b) with $uv_d>0$ is tilt unstable yielding a long-lived anticyclonic monopole.

C. Structural stability of Rossby-drift wave vortex structures

In Sec. II we gave the details of the derivation of the nonlinear drift wave equation (2.16) based on the ε expansion in Eq. (2.1) and the corresponding derivation of the quasi-geostrophic nonlinear equation (2.27) for the 2-D flow on the surface of a rotating planet described by Eqs. (2.19)–(2.22). The resulting nonlinear dynamics can be expressed in both cases by the conservation law known as Ertel's theorem [Ertel (1942)]. Ertel's theorem applies to the 2-D motion of the fluid taken from the dynamics of the total system vorticity

$$\left(\frac{\partial}{\partial t}+\mathbf{v}\cdot\nabla\right)(\boldsymbol{\omega}_0+\boldsymbol{\omega})+(\boldsymbol{\omega}_0+\boldsymbol{\omega})\nabla\cdot\mathbf{v}=(\boldsymbol{\omega}_0+\boldsymbol{\omega})\cdot\nabla\mathbf{v},\qquad(5.3)$$

where the plasma $\boldsymbol{\omega}_0=e\mathbf{B}/mc$ and for the planetary problem $\boldsymbol{\omega}_0=\mathbf{f}=2\,(\omega_{\rm rot})_z\hat{\mathbf{z}}$ where $2\pi/\omega_{\rm rot}$ is the period for the rotating planet and $(\omega_{\rm rot})_z=\omega_{\rm rot}\sin\theta$ where θ is the local latitude. The

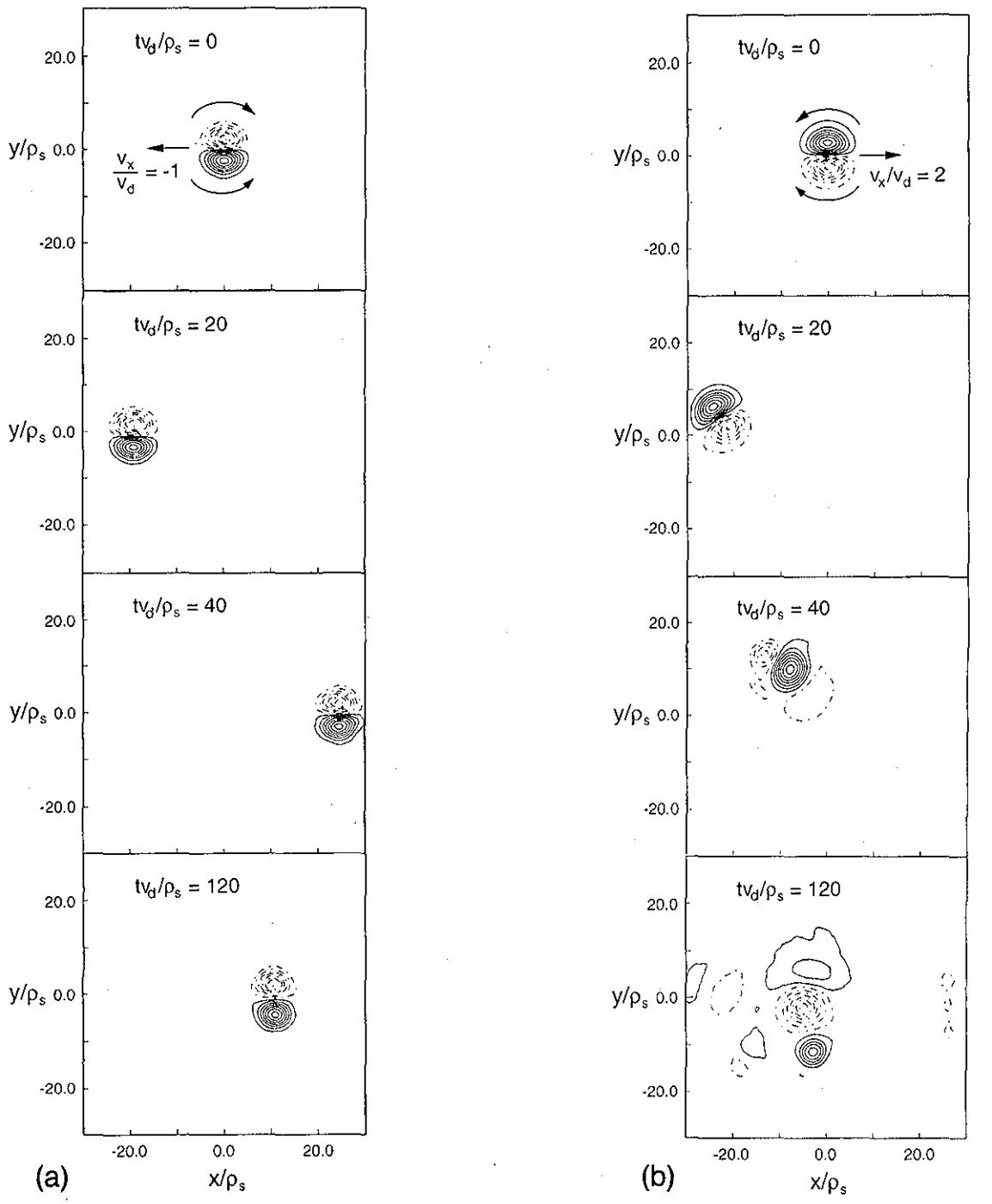

FIG. 10. Comparison of the effect of a 2% monopolar perturbation on dipoles propagating in (a) the eastward direction and (b) the westward direction. For $u=-v_d$ and $a=6\rho_s$, the vortex propagates in the ion diamagnetic direction or eastward Rossby wave and is stable. The same 2% monopolar perturbation applied in frame (b) to the dipole with $u=2v_d$ produces unstable rotation and splitting up into monopolar structures.

right-hand side of Eq. (5.3) is called the vorticity stretching term and couples the vorticity equation for plasmas to the ion-acoustic waves $\omega^2 = k_z^2(T_e/m_i)$ along the magnetic field **B** and for the planetary problem couples the vorticity to vertical gravitational waves known as the internal gravity waves. When (i) the z component of Eq. (5.3) is taken, (ii) the vortex stretching term is neglected, and (iii) the mass conservation law is used to eliminate $\nabla\cdot\mathbf{v}$, we obtain the CHM equation in a form that expresses the conservation of a generalized or potential vorticity $q(x,y,t)$ where

$$\frac{dq}{dt}=\left(\frac{\partial}{\partial t}+\mathbf{v}\cdot\nabla\right)q=0 \tag{5.4}$$

with

$$q=\frac{\omega_{ci}+\omega_z}{n}=\frac{\omega_{ci}(1+\nabla^2\phi)}{n_0(x)\ \exp\ (e\phi/T_e)} \tag{5.5}$$

for plasmas and

$$q=\frac{f+\hat{\mathbf{z}}\cdot\nabla\times\mathbf{v}}{H}=\frac{f\ (1+\nabla^2 h)}{H_0(x,y)+h(x,y,t)} \tag{5.6}$$

for quasigeostrophic planetary flows. It is not difficult to show that both Eqs. (2.16) and (2.27) are equivalent to Eq. (5.4) with Eq. (5.5) or (5.6) for q, respectively.

Expressing the CHM equation as the conserved flow of the generalized vorticity q is important for deriving the effect of small changes in the form of the equation. In addition the conservation form (5.4) makes clear that there is a general class of invariants of the motion called Casimirs [Kandrup and Morrison (1993)] that are given by any function $F(q)$ integrated over all space, or over a periodic box,

$$\frac{\partial}{\partial t}\int dx\ dy\ F(q)=0 \tag{5.7}$$

in the dissipationless limit. These Casimirs may be thought of as restricting the dynamics in function space to lie on fixed sheets defined by the value of $C=\int dx\ dy\ F(q)$.

The existence of the Casimir invariants is a reflection of the Hamiltonian structure of the dynamical system and does not imply integrability. Piterbarg and Schulman (1989) address the issue of integrability of the CHM equation. They claim to show that there are no invariants of the CHM motion other than the Casimirs and the standard energy W and momenta (P_x, P_y) invariants (or equivalently the energy W, enstrophy U and the P_x momentum). It is then argued that the nonexistence of further invariants implies the nonintegrability of the CHM equation. The arguments are technically complex and follow the method of Zakharov and Schulman (1988) which is based on a continuum field generalization of the well-known Poincaré approach for the investigation of the integrability of finite number of degrees of freedom Hamiltonians. Further consideration of the integrability issue is given in Piterbarg and Schulman (1989).

From Eqs. (5.4)–(5.6) we now consider the effect of weak spatial inhomogeneities in the system that give rise to a well-studied structural perturbation (or change in form) of the CHM equation. The modification to the CHM equation is to add the nonlinear term $\phi\partial_y\phi$ known alternatively as the Korteweg–de Vries (KdV) nonlinearity or the scalar nonlinearity to contrast its form from the $\hat{\mathbf{z}}\cdot\nabla\phi\times\nabla q$ vector (or Poisson bracket) nonlinearity. Both types of nonlinearities ($\phi\partial_y\phi$ and $\hat{\mathbf{z}}\cdot\nabla\phi\times\nabla\nabla^2\phi$) have been extensively studied and are known to be characteristic of Hamiltonian field equations [Morrison (1982)].

The most important aspect of the change in the CHM equation from the weak inhomogeneity can be described by adding the Korteweg–de Vries term with the variable perturbation parameter α so that the model equation is

$$(1-\nabla^2)\frac{\partial\phi}{\partial t}+v_d\frac{\partial\phi}{\partial y}+\alpha\phi\frac{\partial\phi}{\partial y}+[\nabla^2\phi,\phi]=0. \tag{5.8}$$

Even for very small α this new equation has a qualitatively different behavior in the long time limit due to the existence of new solitary waves that have peak amplitude varying as $1/\alpha$.

The sign of the peak is determined by the sign of α which we allow to carry its algebraic sign in Eq. (5.8) and in the subsequent analysis. In the rotating parabolic water tank experiments α is opposite in sign to that of the usual plasma regime in which the sign of α is determined by the ratio of the electron-to-density gradient parameter $\eta_e=\partial_r \ln T_e/\partial_r \ln n_e$. The difference in the sign of α will change the preferred solitary wave structure from anticyclonic to cyclonic as discussed by Nezlin and Snezhkin (1993). In the plasma the sign of the structure is important in its tendency to trap ions or electrons in the motion parallel to the magnetic field [Jovanović and Horton (1993b)].

In the study of nonlinear drift waves, equations of the 1-D limit of Eq. (5.8), which is

$$(1-\partial_y^2)\frac{\partial\phi}{\partial t}+v_d\frac{\partial\phi}{\partial y}+\alpha\phi\frac{\partial\phi}{\partial y}=0, \tag{5.9}$$

were discovered before the Hasegawa–Mima equation by Tasso (1967) by studying the effect of a temperature gradient $T_e(x)$. The coefficient is $\alpha=-v_d\eta_e$ where $\eta_e=d\ \ln T_e/d\ \ln n_0$. Equation (5.9) is closely related to the classical KdV equation by considering the long wavelength limit where $(\partial_t+v_d\partial_y)\phi\approx 0$ and then replacing the term $\partial_y^2\partial_t\phi$ with $-v_d\partial_y^3\phi$ retrieves the classical KdV equation. Thus, Eq. (5.9) is sometimes called the modified KdV equation or MKdV. The modified KdV equation is important from the physical point of view since it has solitary waves and quasielastic scattering but only a few polynomial invariants of the motion and no inverse scattering theory. Thus, the modified KdV equation is closer in kind to the CHM equation than the classical KdV equation which has an infinite sequence of polynomial invariants and an exact solution of the initial value problem given by inverse scattering theory.

The fluctuation spectrum and other dynamical characteristics of the one-dimensional multiple-solitary wave dynamics produced by Eq. (5.9) is reported in Meiss and Horton (1992).

D. Splitting of dipolar vortex into monopoles

Now we consider the physical role of the KdV term. By combining the coefficients of the $\partial\phi/\partial y$ terms in Eq. (5.8) we see that effective spread of propagation of a structure is

$$\frac{dy}{dt}=v_d+\alpha\phi \tag{5.10}$$

so that regions with $\alpha\phi/v_d>0$ propagate faster than v_d, while regions with $\alpha\phi/v_d<0$ propagate slower than v_d.

Considering the dipole vortex solution of Sec. II C we now see that the positive and negative vortex lobes propagate with different speeds. Studies by Su *et al.* (1991) show that the speeds of the positive and negative centers are $u_\pm\cong v_d\pm\alpha|\phi_{\rm dp}|/4.8$ so that in time Δt the relative speeds u_+-u_- separate the two dipole lobes by its own diameter $2r_0$ where

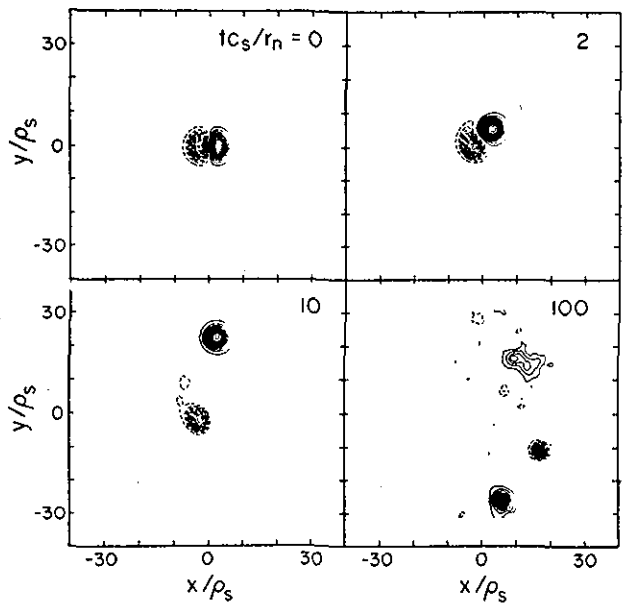

FIG. 11. Splitting drift wave dipole vortex into monopoles. Dipole radius $r_0=6\rho_s$, amplitude of scalar nonlinearity $\alpha=0.1(\eta_e\rho_s/r_n)$, and vortex velocity $u=2v_d(v_d=1)$. At $t=0$, (a) shows the contours for the exact dipole vortex solution of the Hasegawa–Mima–Rossby wave Eq. (2.16). The solid lines represent positive value of potential ϕ, and the dashed lines, negative value. The contours for ϕ have contour interval $\Delta\phi=4.0$.

$$\Delta t=\left(\frac{4.8}{2}\right)\frac{r_0}{\alpha v_d|\phi_{\rm dp}|}. \tag{5.11}$$

After time Δt the dipoles are split into monopoles and both signs will propagate for a period depending on the strength of the vortices. In the presence of the α term, however, there is a preferred sign for vortex self-binding. So after some number of rotation periods only the preferred sign monopole will survive.

An example of the dipole vortex splitting from Su *et al.* (1991) is shown in Fig. 11 for $\alpha=0.1$. In the last time frame the long-lived, anticyclonic vortex has been formed and continues to propagate for a long time. The long-lived anticyclonic vortices produced by this KdV or scalar nonlinearity appear to be the explanation for the preferential existence of the anticyclones in the experiments of Antipov *et al.* (1982) and Nezlin (1986).

Now we show the existence of the monopolar vortex solution with the sign (cyclone $\phi<0$ versus anticyclone $\phi>0$) determined by the sign of α. The type of monopolar vortex given here was first derived by Petviashvili (1977) and proposed as a model for the Giant Red Spot vortex on Jupiter [Petviashvili (1980)]. The model equation is derived by Petviashvili by keeping nonlinear terms in the expansion of $q(\phi)$ or $q(h)$ in Eq. (5.4).

In contrast to the planetary geostrophic dynamics and the rotating parabolic tank experiments, the University of Texas rotating water tank has a strictly linear dependence of potential vorticity q on the streamfunction $h(x,y,t)$. The linearity arises from the fixed, rigid upper lid on the vessel and the β effect is produced by the slope $(s=dz/dr=-0.1)$ of the bottom of the tank. In this system $q(h)=(f_0+\nabla^2 h)/(H_0-sy)$ which gives $q=\nabla^2 h+\beta y$ with $\beta=f_0\,s/H_0$. As shown by del-Castillo-Negrete and Morrison (1993) the nonlinear dynamics is solely governed by the nonlinear convective derivative. In these experiments the preference for cyclonic or anticyclonic vortices occurs from the direction of pumping which produces either an eastward or westward (Bickley) jet $U_0\,\mathrm{sech}^2(y/L)$ with the associated shear flow instability for $U/L^2>\beta=f_0 s/H_0$.

E. Monopolar vortices from the KdV-term in the *generalized CHM equation*

When the amplitude ϕ_m of a coherent structure is large enough that the rotation rate Ω_v around the local maximum $\phi_m(1-r^2/r_0^2)$ of the potential, or h function, given by

$$\Omega_v=\frac{1}{r}\frac{d\phi}{dr}=-\frac{2\phi_m}{r_0^2} \tag{5.12}$$

exceeds the corresponding wave frequencies, $\omega_k=k_y v_d\sim\pi v_d/r_0$. When $\Omega_v>\pi v_d/r_0$ then the convective nonlinearity in the CHM equation forces the coherent structure to be nearly axisymmetric, $\phi=\phi_0(r)+\phi_1(r)\cos\theta$ with $\phi_1\ll\phi_0$.

Now we look for exactly axisymmetric solutions in the frame moving with the structure

$$\phi(x,y,t)=\phi_0(r) \tag{5.13}$$

with

$$r=[x^2+(y-ut)^2]^{1/2},$$
$$\theta=\tan^{-1}\left(\frac{y-ut}{x}\right).$$

Since $\hat{\mathbf{z}}\cdot\nabla\phi\times\nabla f=r^{-1}(\phi_\theta f_r-\phi_r f_\theta)$ vanishes for $\phi(r)$ and $f=\omega(r)=\nabla^2\phi=r^{-1}\partial_r(r\partial_r\phi)$, Eq. (5.8) reduces to

$$-u(1-\nabla^2)\frac{\partial\phi}{\partial y}+u_d\frac{\partial\phi}{\partial y}+\alpha\phi\frac{\partial\phi}{\partial y}=0$$

for which integration in y yields the nonlinear elliptic equation

$$\nabla^2\phi=\frac{1}{r}\frac{d}{dr}\left(r\frac{d\phi}{dr}\right)=k^2\phi-\frac{\alpha}{2u}\phi^2, \tag{5.14}$$

where

$$k^2=1-\frac{v_d}{u}. \tag{5.15}$$

For $k^2>0$ $(u>v_d$ or $uv_d<0)$ as in the dipolar solution we have the exponentially decaying Bessel function solution $\phi\sim\phi_e K_0(kr)\sim e^{-kr}/\sqrt{r}$ for $|\phi|\ll 2uk^2/\alpha$. The presence of the α term allows solutions with the sign of ϕ the same as the sign of uk^2/α to change from positive to negative curvature, and thus to form bound nonlinear states for sufficiently large $\phi(r=0)>2uk^2/\alpha$. Mathematically, finding the physically acceptable solutions of Eq. (5.14) poses a nonlinear eigenvalue problem which has been solved analytically and numerically by Su *et al.* (1991).

The solutions of (5.14) are well approximated by

$$\phi=\frac{4.8uk^2}{\alpha}\left[\operatorname{sech}\left(\frac{3}{4}k[x^2+(y-ut)^2]^{1/2}\right)\right]^{4/3}. \quad (5.16)$$

This approximate solution given by Petviashvili and Pokhotelov (1986) is found by constructing a variational principle with the trial solution $\phi_{\max}[\operatorname{sech}(kr/p)]^p$ which matches the asymptotic form $kr\gg 1$ of e^{-kr} and has $\phi\simeq\phi_m(1-r^2/r_0^2)$ for $r\to 0$. The parameters $\phi_{\max}$ and p are determined by the variational formulation of Eq. (5.14) and the boundary conditions. The relation $\phi_{\max}=4.8uk^2/\alpha$ gives the speed of the vortex as $u=v_d(1+\alpha\phi_{\max}/4.8)$ which explains the observed dipole splitting discussed in Sec. V D. The sign of the structure $\phi_{\max}$ is determined by the sign of α.

F. Generalized vortex dynamical models

The model equation (5.8) with only the addition of the KdV term, while clearly useful and of historical interest, is not consistent with Ertel's theorem and has been the subject of considerable debate during the past five years. The equation of this form was originally given by Petviashvili (1977) and is often called the Petviashvili equation. The inconsistency of the Petviashvili equation with the conservation of potential vorticity, or Ertel's theorem, has been the subject of recent works by Lakhin *et al.* (1987), Horihata and Sato (1987), Nycander (1992), Spatschek *et al.* (1990), and Su *et al.* (1991). Even much earlier the basic difficulty can be seen from comparison of the Petviashvili model equation with the systematic derivation of these terms in the works of Willliams (1978) and (1985). Finally, the recent work of Spatschek *et al.* (1990) claims to have systematically obtained the Petviashvili model by introducing a rather special ordering of the space–time scales. Basically the idea is to compare the space scale length L dependencies of the contributions of $\alpha\phi\,\partial\phi/\partial y\sim\alpha\phi^2/L$ with those from $\nabla\phi\times\nabla\nabla^2\phi\sim\phi^2/L^4$. We see that for large-scale structures the KdV dominates the vector nonlinearity. Thus Spatschek *et al.* propose a particular ordering for which the model Eq. (5.9) is the leading order equation for large-scale (ρ_g/ϵ) structures where ϵ is a particular small expansion parameter.

In the late work of Petviashvili he recognized the difficulty and derived the consistent model by using Eq. (5.4) for the conservation of the potential vorticity which is itself expanded in powers of h and the inhomogeneity y. The CHM equation then is the lowest order equation obtained from the linear part of the potential vorticity $q^l=\nabla^2h-h+\beta y$. The generalized nonlinear potential vorticity is

$$q=\nabla^2h-h+\beta y+q^{nl},$$
$$q^{nl}=-\beta yh+h^2-\frac{|\beta'|y^2}{2}, \quad (5.17)$$

which is readily derived by expanding $q=(f+\nabla^2h)/(1+h)$ with $f=1+\beta y-|\beta'|y^2/2$ up to second order in y and h. The dynamical equation $dq/dt=0$ now gives rise to both the vector nonlinearity and the KdV nonlinearity as well as a nonlocal dependence in y of the coefficients of the nonlinear partial differential equation. For the planetary problem of radius r_0 at latitude θ_0 the values are $\beta=(\rho_g/r_0)\cot\theta_0$ and $|\beta'|\cong(\rho_g/r_0)^2$ with the amplitude of the solitary monopole in Eq. (5.16) given by $h_{\max}\simeq 4.8(u+\beta)/\beta$. For small height perturbations $|h|<1$ this requires $u\beta<0$ and $|u/\beta+1|<1/5$.

The same problem occurs with the plasma equation and is dealt with in the same manner. If we begin with Eqs. (5.4) and (5.5), and recognize that the temperature profile $T_e=T_e(x)$ determines the gradient of $v_d(x)$ across the diameter of the vortex, then we arrive at the equation

$$\left(\frac{1}{T(x)}-\nabla^2\right)\partial_t\phi+v_d\frac{\partial\phi}{\partial y}+\kappa_T\phi\frac{\partial\phi}{\partial y}+[\nabla^2\phi,\ \phi]=0, \quad (5.18)$$

where $T(x)=T_e(x)/T_0$, $\kappa_T=\rho_{s0}T'(x)/T^2(x)$, and $\phi=(r_n/\rho_{s0})\,(e\Phi/T_0)$, $v_d=-(cT_0/eB)d\ln n_0/dx$. Here space and time derivatives are normalized by ρ_{s0} and r_n/c_{s0}, respectively, and are defined by the temperature $T_e(x=0)=T_0$ at the center of the vortex.

In the geophysical literature essentially the same equation (5.18) is derived for the so-called intermediate geostrophic dynamics which applies to larger scale dynamics than the CHM, or quasigeostrophic equation, as discussed by Williams (1985).

G. Propagation and collisions of the monopole vortices

For the vortex–vortex interactions we have established from numerical simulations that the monopole vortices that evolve from Eq. (5.18) with the initial data from (5.16) can behave under collisions as either

(1) soliton-like collisions with the stronger vortex overtaking and passing through the weaker vortex; or

(2) point vortex-like interactions where two strong monopole vortices, which by Eq. (5.16) are always of the same sign, rotate about one another.

In Fig. 12 we show an example of the soliton-like pass-through collision. In Fig. 13 we show an example of the second case where two nearly equal strength monopole vortices interact like point vortices rotating around one another.

Wave radiation occurs from the monopolar vortices. As the amplitude ϕ_m of the vortices becomes small, the speed of propagation in Eq. (5.16) approaches the linear wave speed and the coupling to the wave field radiates energy from the vortex. Su *et al.* (1991) calculate this radiative decay of the vortex. The local energy conservation equation is

$$\frac{\partial\varepsilon}{\partial t}+\nabla\cdot\mathbf{S}=0, \quad (5.19)$$

where

$$\varepsilon(x,y,t)=\frac{1}{2}\left[\frac{\phi^2}{T(x)}+(\nabla\phi)^2\right] \quad (5.20)$$

and the "Poynting" energy flux is

$$\mathbf{S}=\left(\frac{1}{2}v_d(x)\phi^2-\frac{1}{3}\kappa_T\phi^3\right)\hat{\mathbf{y}}-\phi\nabla\frac{\partial\phi}{\partial t}$$
$$-\nabla^2\phi\hat{\mathbf{z}}\cdot\nabla(\phi^2/2). \quad (5.21)$$

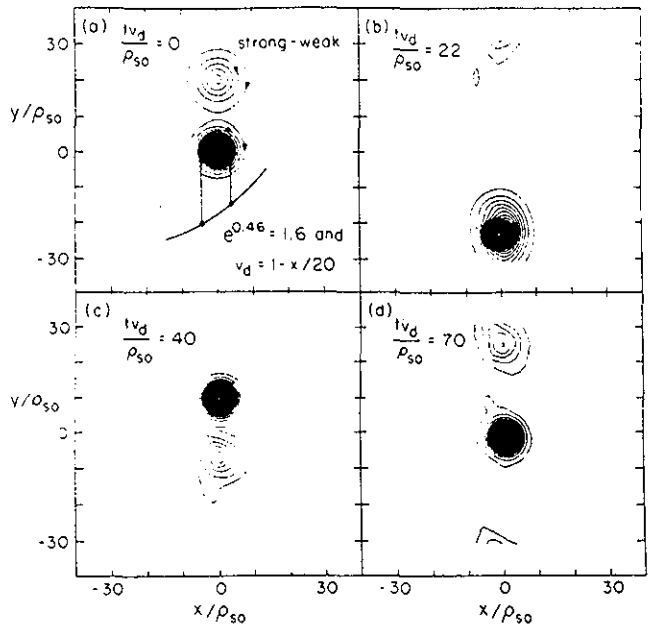

FIG. 12. Nearly elastic overtaking collision of a strong monopole vortex with a weaker monopole. The profile of $1/T(x)=1/L_d^2=\exp(0.46x)$ gives a variation of 1.6 over the core of the vortex. The gradient in the drift-Rossby speed is $v_d(x)=1-x/20$. The solution conserves $q=\nabla^2\phi-\phi/T(x)+\int^x v_d\,dx'$. The speeds are $u_1=1.1$ and $u_2=1.7$ giving the expected collision time $\Delta l/\Delta u=20/0.6=33$ compared with observed overlapping at $t=22$ in frame (b). After separation [(c) and (d)] the weaker vortex still has five closed contours.

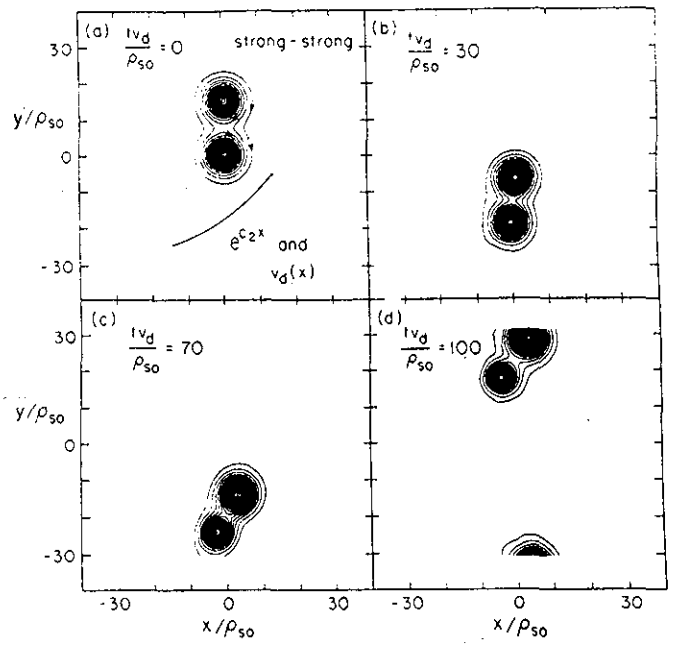

FIG. 13. Point vortex type of interaction of two strong monopole vortices with speeds $u_1=1.3$ and $u_2=1.35$. Although merging might be expected here, instead the vortices rotate around one another after pulling together from the initial separation of $15\rho_s$.

The results of a lengthy calculation are that the decay of the vortex energy

$$E_v=\int \varepsilon\, d^2x=\frac{8.2\pi u^4 k_0^2}{(v'_{d0})^2}\left(\frac{4}{3}+k_0^2\right) \tag{5.22}$$

is given by

$$\frac{dE_v}{dt}\cong-\frac{u|\alpha|\phi_m^2}{16\pi\, k_0^3}\exp\left(-\frac{4(1-v_d/u)^{3/2}}{3|\alpha|}\right), \tag{5.23}$$

where $v_{d0}=v_d(x=0)$, $v'_{d0}=dv_d(x)/dx$ and $\alpha=(\kappa_T-v'_{d0}/u)$. The exponential decay factor is controlled by the strength of the inhomogeneity through α [Eq. (5.18)] and the closeness of the speed of propagation u to the drift speed v_d evaluated at the center of the vortex. Simulations for $k_0^3\gg\alpha$ and $k_0^3\ll\alpha$ are shown in Su *et al.* (1991).

The decay of the vortex amplitude in Eq. (5.23) via the coupling to the radiation field will cause the speed u to decrease through Eq. (5.22), and as the speed $u(t)$ decreases the vortex decay rate increases exponentially through Eq. (5.23). Thus, the vortex will decay slowly initially and then suffer an abrupt death.

In the case of magnetic shear, which is another form of inhomogeneity that gives rise to a coupling to vertical v_z oscillations, Meiss and Horton (1983) show that the decay rate of the dipole vortex soliton is given by

$$\frac{dE_{\rm dp}}{dt}=-2\phi_m^2\frac{L_n}{L_s}\left(1-\frac{v_d}{u}\right)^{-1/2}\exp\left[-\frac{\pi L_s}{2L_n}\left(1-\frac{v_d}{u}\right)\right], \tag{5.24}$$

where L_s/L_n is magnetic shear (inhomogeneity) length over the density gradient scale length L_n. Equation (5.24) is an important example of how the "self-organized" nonlinear state can greatly reduce or eliminate the effect of the inhomogeneities L_s/L_n on the waves. When the speed parameter u/v_d is negative (eastward) or not too close to one then the decay rate of the vortex becomes exponentially small. Thus, while small amplitude drift waves have strong shear damping rates the large amplitude vortices can have very long lifetimes.

The vortex structures appear to be a natural or "self-organized" way in which the plasma can feed upon the free energy available in the density gradient and limit the radiation damping inherent in small amplitude waves. Recent simulations indicate that the vortex localization process in systems with rather different linear growth rates (due to damping caused by magnetic or velocity shear) can end up in similar final turbulent states when enough energy is fed into the system. This is because the localization to vortex structures essentially eliminates the shear damping mechanisms. This nonlinear dynamics and the shear damping introduces a form of hysteresis into the system, due to the slow decay rate of the vortices once they are formed. An example of the 2-D vortex in a sheared magnetic field with coupling to the ion-acoustic waves is given in Fig. 14.

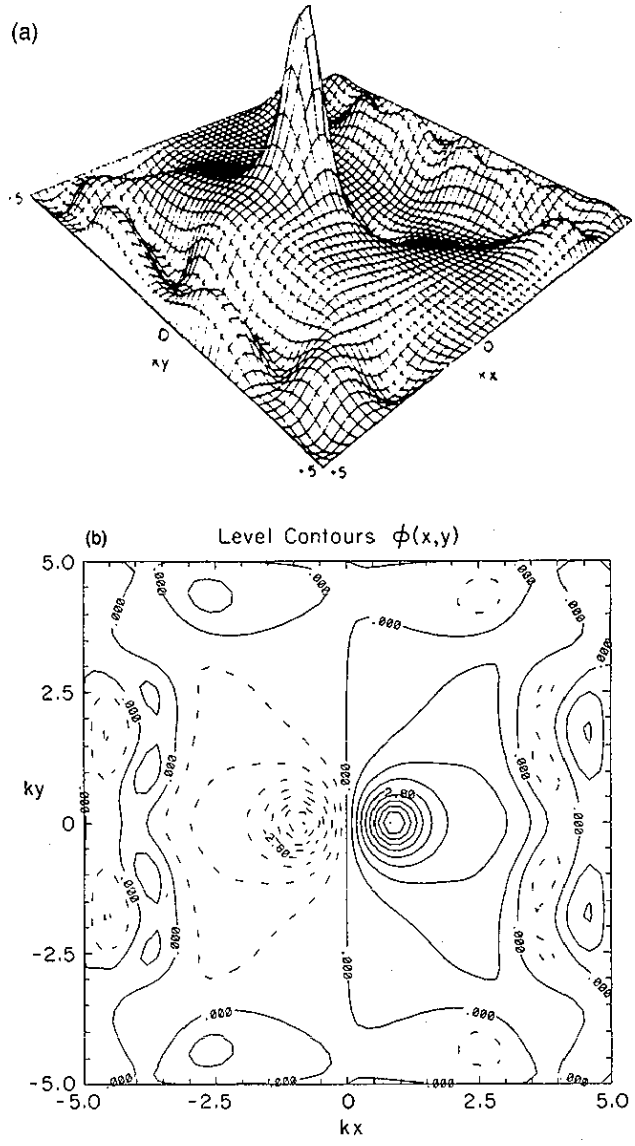

FIG. 14. Drift wave–ion-acoustic wave vortex in a sheared magnetic field for $s=1$. (a) 3-D plot. (b) Contour plot.

H. Driving of the large-scale vortex structures and shear flows by the small-scale Rossby-drift wave turbulence

Finally, we consider the interaction of the small-scale, weakly correlated Rossby-drift wave fluctuations

$$\phi \text{ (small scale)} \rightarrow \psi = \sum_{\mathbf{k}} \psi_{\mathbf{k}}(\varepsilon \mathbf{x}, \varepsilon t) e^{i\mathbf{k}\cdot\mathbf{x} - i\omega_{\mathbf{k}} t}$$

with

$$\langle \psi_{\mathbf{k}}(\varepsilon \mathbf{x}, \varepsilon t) \psi_{\mathbf{k}'}(\varepsilon \mathbf{x}, \varepsilon t) \rangle = \frac{\delta_{\mathbf{k},\mathbf{k}'} N_{\mathbf{k}}(\mathbf{X}, T)}{1 + k_{\perp}^2}, \tag{5.25}$$

where the wave density $N_{\mathbf{k}}(\mathbf{X},T)$ with $\mathbf{X}=\varepsilon\mathbf{x}$, $T=\varepsilon t$ satisfies the kinetic equation

$$\frac{\partial N_{\mathbf{k}}}{\partial T} + \frac{\partial \tilde{\omega}_{\mathbf{k}}}{\partial \mathbf{k}} \cdot \frac{\partial N_{\mathbf{k}}}{\partial \mathbf{X}} - \frac{\partial \tilde{\omega}_{\mathbf{k}}}{\partial \mathbf{X}} \cdot \frac{\partial N_{\mathbf{k}}}{\partial \mathbf{k}} = 2\gamma_{\mathbf{k}} N_{\mathbf{k}} + T_{\mathbf{k}}^{nl}(N_{\mathbf{k}}, N_{\mathbf{k}'}) \tag{5.26}$$

with $T_{\mathbf{k}}^{nl}$ given in Eq. (4.6) and the local drift wave frequency depends on the large-scale ϕ_L, $\tilde{n}_L$ variations through

$$\tilde{\omega}_{\mathbf{k}} = \mathbf{k}\cdot\hat{\mathbf{z}}\times\nabla\phi_L + \frac{\mathbf{k}\cdot\hat{\mathbf{z}}\times\nabla(n_0+\tilde{n}_L)}{1+k_{\perp}^2} \tag{5.27}$$

with large-scale motions governed by ϕ (large scale)$\rightarrow\phi(X,Y,T)$ that satisfies the CHM equation containing the average of $\langle\{\psi,\nabla^2\psi\}\rangle$ over the small-scale turbulence. The driven large-scale CHM equation is given by

$$(1-\nabla^2)\partial_T\phi + v_d\partial_Y\phi - \{\phi,\nabla^2\phi\} = (\partial_X^2 - \partial_Y^2)A + \partial_{XY}^2 B, \tag{5.28}$$

where

$$\begin{bmatrix} A(X,Y,T) \\ B(X,Y,T) \end{bmatrix} = \sum_{\mathbf{k}} \begin{bmatrix} (k_x k_y) \\ (k_x^2 - k_y^2) \end{bmatrix} \frac{N_{\mathbf{k}}(X,Y,T)}{1+k_{\perp}^2}. \tag{5.29}$$

The two-scale equations (5.26)–(5.29) are derived in Dyanchenko *et al.* (1992) and Horton and Petviashvili (1993). In this approach the small-scale turbulence is considered to consist of a number density $N_k(\mathbf{X},T)$ of high frequency quanta moving on the background of a mean shear flow formed by the large-scale motions. Dyachenko *et al.* (1992) point out that the description is similar to that of the superfluid He^4 as a mixture of two fluids as the spectrum of small-scale rotons in the large-scale phonons. They also propose that the system may be solved numerically by modifying the standard particle-in-cell (PIC) codes with the drift wave kinetic equation replacing the particle Vlasov equation. This system of equations leads to the modulational growth of large-scale structures from the inhomogeneity of the distribution of the small-scale fluctuations [Shapiro *et al.* (1993)]. In a tokamak the small-scale turbulence is known to have a strongly increasing strength toward the low density side and, at a given radius, an increase in strength toward the outside of the torus compared with the inside. In planetary atmospheric turbulence it may be expected that the intensity of the small-scale turbulence is stronger in the equatorial zones than in the high latitude regions. It is clear from the structure of Eqs. (5.27)–(5.29) that when the basic assumptions of the scale separations are satisfied, that anisotropy and inhomogeneity in the small-scale turbulence is a driving force on the large-scale structures. In Sec. IV we have discussed the propagation of the small-scale turbulence by the nonlinear wave kinetic equation (4.6) through nonlocal interactions with the background flow. The separation of space–time scales appears to be an effective method for extending the study of Rossby-drift wave turbulence to more realistic inhomogeneous turbulent states compared with the previously studied homogeneous turbulent states.

In summary we note that the importance of the α-KdV term and other nonlocal effects depends on the size of the cyclones and anticyclones. In the Earth's atmosphere the size in terms of the Rossby radius depends on the latitude as given by $\rho_g=(H_0g)^{1/2}/f=2\times10^6$ m/sin θ where θ is the angle of latitude, the equilibrium depth $H\cong10^4$ m, the speed $c_g=(gH)^{1/2}\simeq300$ m/s, and $\beta=0.3\cot\theta$, $R_p=6.4\times10^6$ m. On the gaseous outer planets the vortex structures are usually anticyclones larger than ρ_g. For example, the Great Red Spot on Jupiter is estimated to be $3\rho_g$. In plasmas, the peak of the wave-number spectrum in some tokamak μ-wave scattering experiments is at $k_\perp\approx3$ cm^{-1} and $\rho_s=0.1$ cm giving $k_\perp\rho_s=0.3$. If the fluctuations are associated with vortices such that $k_\perp r_0\lesssim\pi$, then the inferred radius is $r_0\lesssim10\rho_s$ or about 1 cm. In other experiments the fluctuation spectrum appears to increase monotonically down to the small $k_\perp\approx1$ cm^{-1} available from microwave scattering. Attempts to find direct evidence of vortex structures have not been successful in the toroidal confinement experiments. In small, steady-state Q-machine experiments, however, vortices of size $3\rho_s$ have been measured in the shear flow boundary layer of these cylindrical plasmas [Pécseli *et al.* (1984, 1985)] and [Huld *et al.* (1991)].

ACKNOWLEDGMENTS

The work done by one of the authors (WH) was partially supported by U. S. Department of Energy Contract No. DE-FG05-80ET-53088, while that done by the other author (AH) was supported by a Grant-in-Aid for Specially Promoted Research of the Ministry of Education, Science and Culture of Japan.

Antipov, S.V., Nezlin, M. V., Snezhkin, E. N., and Trubrikov, A. S., Zh. Eskp. Teor. Fiz. **82**, 145 (1982) [Sov. Phys. JETP **55**, 85 (1982)].
Antonova, R. A., Zhvaniya, P. B., Lominadze, D. K., Nanobashvili, Dzh., and Petviashvili, V. I., Pisma Zh. Eksp. Teor. Fiz. **37**, 545 (1983) [JETP Lett. **37**, 651 (1983)].
Balk, A. M., Zakharov, V. E., and Nazarenko, S. V., Sov. Phys. JETP **71**, 249 (1990).
Balk, A. M., and Nazarenko, S. V., Sov. Phys. JETP **70**, 1031 (1990).
Balk, A. M., Nazarenko, S. V., and Zakharov, V. E., Phys. Lett. A **146**, 217 (1990).
Balk, A. M., Nazarenko, S. V., and Zakharov, V. E., Phys. Lett. A **152**, 276 (1991).
Behringer R. P., Meyers, S. D., and Swinney, H. L., Phys. Fluids A **3**, 1243 (1991).
Bravenec, R. V., Gentle, K. W., Richards B., Ross, D. W., Sing, D. C., Wootton, A. J., Brower, D. L., Luhmann Jr., N. C., Peebles, W. A., Yu, C. X., Crowley, T. P., Heard, J. W., Hickok, R. L., Schoch, P. M., and Zhang, X. Z., Phys. Fluids B **4**, 2127 (1992).
Brower, D. L., Peebles, W. A., Luhmann, N. C., Phys. Rev. Lett. **54**, 689 (1985).
Charney, J. G., Geophys. Public. Kosjones Nors. Videnskap. Akad. Oslo **17**, 3 (1948).
Del-Castillo-Negrete, D., and Morrison, P. J., Phys. Fluids A **5** 948 (1993).
Dyanchenko, A. I., Nazarenko, S. V., and Zakharov, V. E., Phys. Lett. A **165**, 330 (1992).
Ertel, H., Meterofol. Zh. **59**, 277 (1942).
Flierl, G. R., Larichev, V. D., McWilliams, J. C., and Reznik, G. M., Dyn. Atmos. Oceans **5**, 1 (1980).
Gordin, V. A., and Petviashvili, V. I., Dokl. Akad. Nauk. SSSR **285**, 857 (1985) [Sov. Phys. Dokl. **30**, 1004 (1985)].
Hasegawa A., and Mima, K., Phys. Rev. Lett. **39** 205 (1977).
Hasegawa, A., and Mima, K., Phys. Fluids **21**, 87 (1978).
Hasegawa, A., Imamura, T., Mima, K., and Taniuti, T., J. Phys. Soc. Jpn. **45**, 1005 (1978).
Hasegawa, A., Maclennan, C. G., and Kodama, Y., Phys. Fluids **22**, 2122 (1979).
Hasegawa, A., and Wakatani, M., Phys. Rev. Lett. **50**, 682 (1983).
Hasegawa, A., and Wakatani, M., Phys. Rev. Lett. **59**, 1581 (1987).
Hendel, H. W., Chu, T. K., and Politzer, P. A., Phys. Fluids **11**, 2426 (1968).
Hinton, F. L. and Horton, C. W., Phys. Fluids **14**, 116 (1971).
Horihata, S., and Sato M., J. Phys. Soc. Jpn. **56**, 2611 (1987).
Horton W., Phys. Rev. Lett. **37**, 1269 (1976).
Horton, W., Choi, D.-I., Terry, P. W., and Biskamp, D., Phys. Fluids **23**, 590 (1980).
Horton, W., Choi, D.-I. and Tang, W. M., Phys. Fluids **24**, 1077 (1981).
Horton, W., Phys. Fluids **29**, 1491 (1986).
Horton W., Tajima, T., and Kamimura, T., Phys. Fluids **30**, 3485 (1987).
Horton W., Phys. Fluids B **1**, 524 (1989).
Horton W., Phys. Rep. **192**, 1 (1990).
Horton W., Su, X. N. and Morrison, P. J., Sov. J. Plasma Phys. **16**, 562 (1991).
Horton, W., and Petviashvili, V., "On the trapping condition for planetary vortex structures," in *Research Trends in Physics: Chaotic Dynamics and Transport in Fluids and Plasmas*, edited by W. Horton, Y. Ichikawa, I. Prigogine, and G. Zaslavsky (American Institute of Physics, New York, 1993).
Horton, W., Dong, J. Q., Su, X. N., and Tajima, T., J. Geophys. Res. **98**, 13377 (1993).
Horton W., Wakatani, M., and Wootton, A. (editors), *Ion Temperature Gradient-Driven Turbulent Transport*, AIP Conf. Proc. 284 (American Institute of Physics, New York, 1994).
Huld, T., Nielsen, A.H., Pécseli, and Juul Rasmussen, J., Phys. Fluids B **3**, 1609 (1991).
Jovanović, D., and Horton, W., Phys. Fluids B **5**, 9 (1993a).

Jovanović, D., and Horton, W., Phys. Fluids B **5**, 443 (1993b).
Kadomtsev, B. B., and Petviashvili, V. I., Dokl. Akad. Nauk SSSR **192**, 754 (1970).
Kandrup, H. E., and Morrison, P. J., Ann. Phys. **225**, 114 (1993).
Kolmogorov, A. N. Dokl. Akad. Nauk. SSR **30**, 301 (1941).
Kono, M., and Miyashita E., Phys. Fluids **31**, 326 (1988).
Kono, M., and Horton, W., Phys. Fluids B **3**, 3255 (1991).
Kraichnan, R. H., Phys. Fluids **10**, 1417 (1967); J. Fluid Mech. **59**, 745 (1967).
Kraichnan, R. H., in *Theoretical Approach to Turbulence*, edited by D. L. Dwoyc, M. Y. Hussain, and R. G. Voigt (Springer, New York, 1989), p. 91
Laedke, E. W., and Spatschek, K. H., Phys. Fluids **29**, 134 (1986).
Laedke, E. W., and Spatschek, K. H., Phys. Fluids **31**, 1442 (1988).
Lakhin, V. P., Mikhailovskii, A. B. and Onischenko, O. E., Phys. Lett. A **199**, 348 (1987); Plasma Phys. Controlled Fusion **30**, 457 (1988).
Larichev, V. D., and Reznik, G. M., Fiz. Plasmy **3**, 270 (1976).
Larichev, V. D., and Reznik, G. M., Oceanology **16**, 547 (1976).
Legras, B., Santangelo, P., and Benzi, R., Europhys. Lett. **5**, 37, (1988).
Makino, M., Kamimura, T., and Taniuti, T., J. Phys. Soc. Jpn. **50**, 980 (1981).
Mazzucato, E., Phys. Fluids **21**, 1062 (1978).
Mazzucato, E., Phys. Rev. Lett. **36**, 792 (1976); **48**, 1828 (1982).
McWilliams, J. C., J. Fluid Mech. **146**, 21 (1984).
McWilliams, J. C., and Zabusky, N. J., Geophys. Astrophys. Fluid Dyn. **19**, 207 (1982); McWilliams, J. C., Flierl, G. R., Larichev, V. D., and Reznik, G. M., Dyn. Atmos. Oceans **5**, 219 (1981).
McWilliams, J. C., Phys. Fluids A **2**, 547 (1990a).
McWilliams, J. C., J. Fluid Mech. **219**, 361 (1990b).
Meiss, J. D., and Horton, W., Phys. Fluids **25**, 1838 (1982).
Meiss, J. D., and Horton, W., Phys. Fluids **26**, 990 (1983).
Mikhailovskii, A. B., Nazarenko, S. V., Novakovskii, S. V., Churicov, A. P., and Onishchenko, O. G., Phys. Lett. A **133**, 407 (1988).
Morikawa, G. Y., J. Meteorol. **17**, 148 (1960).
Morrison, P. J., "Poisson brackets for fluids and plasmas," *in Mathematical Methods in Hydrodynamics and Integrability in Dynamical Systems*, edited by M. Tabor and Y. Treve, AIP Conf. Proc. 88 (AIP, New York, 1982).
Nezlin, M. V., and Snezhkin, E. N., in *Rossby Vortices, Spiral Structures, Solitons* (Springer-Verlag, Berlin 1993), pp. 196–203.
Novakovskii, S. V., Mikhailovskii, A. B., and Onischenko, O. G., Phys. Lett. A **132**, 33 (1988).
Muzylev, S. V., and Reznik, G. M., Phys. Fluids B **4**, 2841 (1992).
Nezlin, M. V., Sov. Phys. Usp. **29**, 807 (1986) [Usp. Fiz. Nauk **150**, 3 (1986)].
Nycander J., Phys. Fluids A **467** (1992).
Onsager L., Suppl. Nuovo Cimento **6**, 279 (1949).
Pécseli, H. L., Juul Rasmussen, J., and Thomsen, K., Phys. Rev. Lett. **52**, 2148 (1984); Plasma Phys. Controlled Fusion **27**, 837 (1985).
Pécseli, H. L., and Trulsen, J., Phys. Fluids B **1**, 1616 (1989).
Pedlosky, J., *Geophysical Fluid Dynamics* (Springer, New York, 1987), pp. 518–532.
Petviashvili, V. I., Fiz. Plazmy **3**, 270 (1977)[Sov. J. Plasma Phys. **3**, 150 (1977)].
Petviashvili, V. I., JETP Lett. **32**, 619 (1980).
Petviashvili, V. I., and O. A. Pokhotelov, Fiz. Plazmy **12**, 651 (1986) [Sov. J. Plasma Phys. **12**, 657 (1986)].
Pierini, S., Dyn. Atmos. Oceans **9**, 273 (1985).
Piterbarg, L. I., and Shulman, E. I., Phys. Lett. A **140**, 29 (1989).
Rudakov, L. I., and Sagdeev, R. Z., Sov. Phys. Dokl. **6**, 415 (1961).
Sagdeev, R. Z., and Galeev, A. A. *Nonlinear Plasma Theory* (Benjamin, New York, 1968).
Scott, B. D., Phys. Fluids B **4**, 2468 (1992).
Shapiro, V. D., Diamond, P. H., Lebedev, V. B., Isoloviev, G., and Shevchenko, V. I., Plasma Phys. Controlled Fusion **35**, 1032 (1993).
Slusher, R. E., and Surko, C. M., Phys. Rev. Lett. **40**, 400 (1978).
Sommeria, J., Meyers, S. D., and Swinney, H. L., "Experiments on vortices and Rossby waves in waves in eastward and westward jets," in *Nonlinear Topics in Ocean Physics*, edited by A. R. Osborne (North-Holland, Amsterdam, 1991), pp. 227–269.
Spatschek, K. H., Laedke, E. W., Marquardt, Chr., Musher, S., and Wenk, H., Phys. Rev. Lett. **64**, 3027 (1990).
Stewart, H. J., Q. Appl. Math. **1**, 262 (1943).
Su, X. N., Horton, W., and Morrison, P. J., Phys. Fluids B **3**, 921 (1991).
Su, X. N., Horton, W., and Morrison, P. J., Phys. Fluids B **4**, 1238 (1992).
Sudan, R. N. and Pfirsch, D., Phys. Fluids **28**, 1702 (1985).
Surko, C. M., and Slusher, R. E., Phys. Rev. Lett. **36**, 1747 (1976).
Swaters, G. E., Phys. Fluids **29** 1419 (1986).
Tasso, H., Phys. Lett. A. **24**, 618 (1967).
Terry, P. W., and Horton, W., Phys. Fluids **25**, 491 (1982).
Terry, P. W., and Horton W., Phys. Fluids **26**, 106 (1983).
Van Heijst, G. J. F., and Flor, J. B., "Laboratory experiments on dipole structures in a stratified fluid," in *Mesoscale/Synoptic Coherent Structures in Geophysical Turbulence*, edited by J. C. J. Nihoul and B. M. Jamart (Elsevier Science, Amsterdam, 1989), pp. 591–608.
Wakatani, M., and Hasegawa, A., Phys. Fluids **27**, 611 (1984).
Wakatani, M., Watanabe, K., Sugama, H., and Hasegawa, A., Phys. Fluids B **4**, 1754 (1932).
Waltz, R. E., Phys. Fluids B **26**, 469 (1983).
Waltz, R. E., Phys. Fluids B **2**, 2118 (1990).
Williams, G. P., J. Atmos. Sci. **35**, 1399 (1978).
Williams, G. P., J. Atmos. Sci. **42**, 1237 (1985).
Zakharov, V. E., "Kolmogorov spectra in weak turbulence problem," *Handbook of Plasma Physics, Vol. II*, edited by M. N. Rosenbluth and R. Z. Sagdeev (Elsevier Science, Amsterdam, 1984), pp. 3–36.
Zakharov, V. E., and Schulman E. I., Physica D **29**, 283 (1988).
Zabusky, N., and McWilliams, J. C., Phys. Fluids **25**, 2175 (1982).

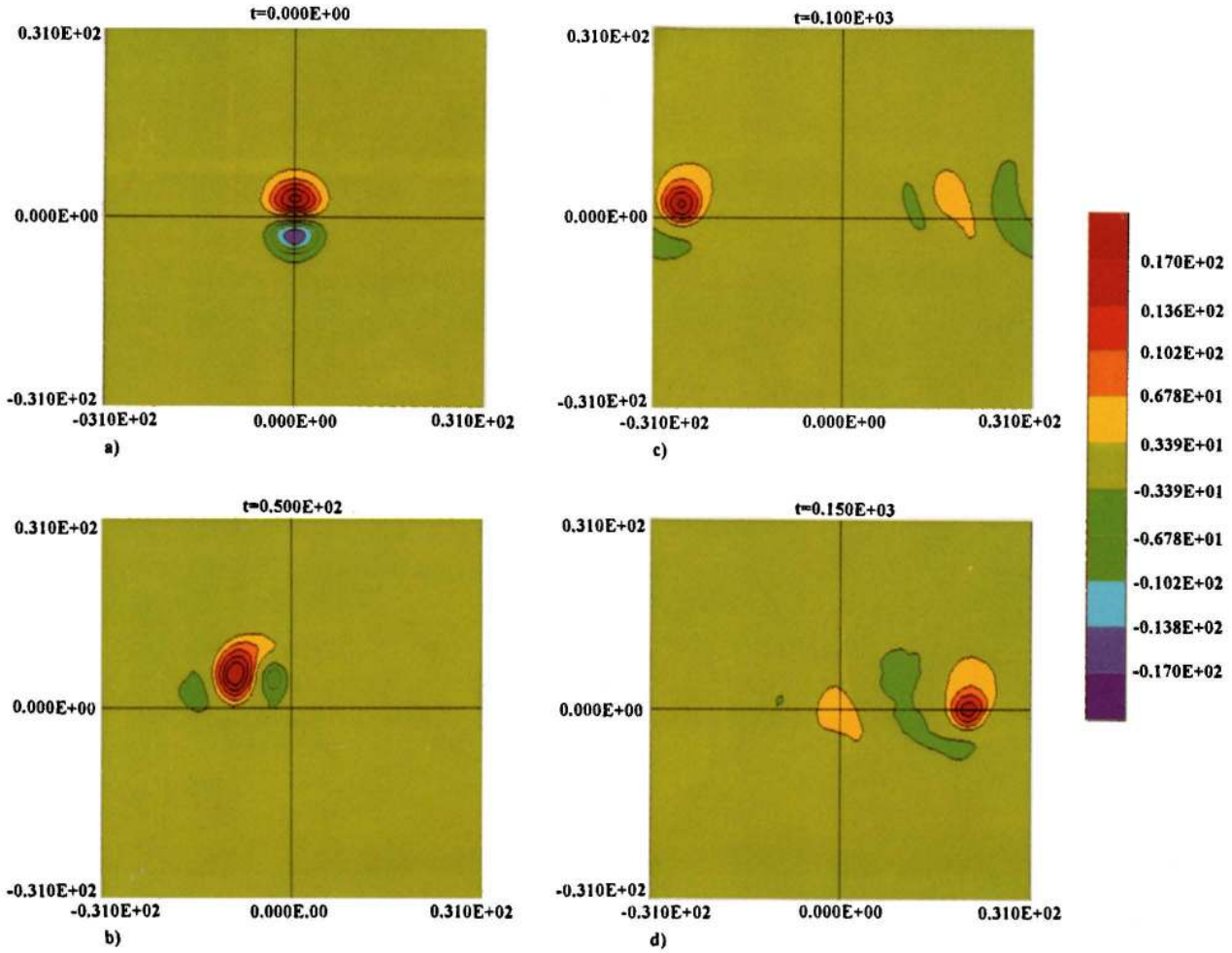

FIG. 9. Typical instability amplitude of the dipole vortex propagating in the direction of the Rossby-drift wave. The initial vortex speed u is $u=1.2v_R$ and the radius is $a=6\rho_s$: a small monopolar perturbation of similar radius is added. The periodic box is $20\pi\rho_s \times 20\pi\rho_s$. The angular rotation frequency in each lobe is $\Omega \simeq 3$ in frame (a) at $t=0$. In frame (b) $tv_R/\rho_s=50$ and the dipole has propagated westward $ut \gtrsim 60\rho_s$ and tilted to approximately 70°. In frame (c) $tv_R/\rho_s=100$ the anticyclone ($\phi>0$) dominates followed by a wake. In frame (d) $tv_R/\rho_s=150$, about 50 rotations after $t=0$, the wake is well separated and the anticyclone with a northward shelf is the surviving long-lived coherent structure.

W. Horton and A. Hasegawa (see page 243)